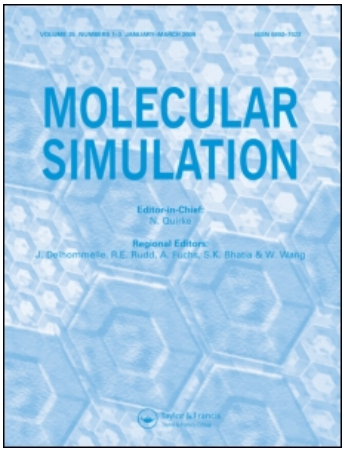

Molecular Simulation
Publication details, including instructions for authors and subscription information:
http://www.informaworld.com/smpp/title~content=t713644482

BioMOCA—a Boltzmann transport Monte Carlo model for ion channel simulation

T. A. van der Straaten[a]; G. Kathawala[a]; A. Trellakis[b]; R. S. Eisenberg[c]; U. Ravaioli[a]
[a] †Beckman Institute for Advanced Science and Technology, University of Illinois, Urbana, IL, USA [b] ‡Walter Schottky Institut (T33), Technische Universitat München Am Coulombwall, Garching, Germany [c] ¶Department of Molecular Biophysics and Physiology, Rush Medical College, Chicago, IL, USA

To cite this Article van der Straaten, T. A. , Kathawala, G. , Trellakis, A. , Eisenberg, R. S. and Ravaioli, U.(2005) 'BioMOCA—a Boltzmann transport Monte Carlo model for ion channel simulation', Molecular Simulation, 31: 2, 151 — 171
To link to this Article: DOI: 10.1080/08927020412331308700
URL: http://dx.doi.org/10.1080/08927020412331308700

Molecular Simulation, Vol. 31, No. 2–3, 15 February–15 March 2005, 151–171

Taylor & Francis
Taylor & Francis Group

BioMOCA—a Boltzmann transport Monte Carlo model for ion channel simulation

T.A. VAN DER STRAATEN†*, G. KATHAWALA†, A. TRELLAKIS‡, R.S. EISENBERG¶§ and U. RAVAIOLI†

†Beckman Institute for Advanced Science and Technology, University of Illinois, 405 N Mathews Avenue, Urbana, IL 61801, USA
‡Walter Schottky Institut (T33), Technische Universitat München Am Coulombwall, D-85748 Garching, Germany
¶Department of Molecular Biophysics and Physiology, Rush Medical College, 1750 W Harrison Street, Chicago, IL 60612, USA

(Received April 2004; in final form July 2004)

With the recent availability of high-resolution structural information for several key ion channel proteins and large-scale computational resources, Molecular Dynamics has become an increasingly popular tool for ion channel simulation. However, the CPU requirements for simulating ion transport on time scales relevant to conduction still exceed the resources presently available. To address this problem, we have developed *Bio*logy *Mo*nte *Ca*rlo (BioMOCA), a three-dimensional (3D) coarse-grained particle ion channel simulator based on the Boltzmann Transport Monte Carlo (BTMC) methodology. Although this approach is widely employed in the engineering community to study charge transport in electron devices, its application to molecular biology and electrolytes in general is new and hence must be validated. The pair correlation function, which is a measure of the microscopic structure of matter, provides a suitable benchmark to compare the BTMC method against the well-established Equilibrium Monte Carlo (EMC) approach. For validation purposes BioMOCA is used to simulate several simple homogeneous equilibrium electrolytes at concentrations of physiological interest. The ion–ion pair correlation functions computed from these simulations compare very well with those obtained from EMC simulations. We also demonstrate several performance-improving techniques that result in a several-fold speed-up without compromising the pair correlation function. BioMOCA is then used to perform full 3D simulations of ion transport in the gramicidin A channel *in situ* in a membrane environment, as well as to study the link between the electrostatic and dielectric properties of the protein and the channel's selectivity.

Keywords: Ion channels; Nanodevices; Gramicidin; Monte Carlo simulations

1. Introduction

Ion channels are a class of proteins that reside in the membranes of all biological cells [1]. Each channel consists of a chain of amino acids folded in such a way that the protein forms a macromolecular aqueous nanopore that conducts ions in and out of the cell. An essential feature of all proteins is that many of the side chains of the amino acids are ionizable, giving rise to a strong permanent charge that varies sharply along the channel. This distribution of charge depends on the physiological environment of the channel, and plays an important role in determining the conduction mechanisms of the open channel. From a physiological point of view, ion channels regulate the transport of ions through the otherwise impermeable cell membrane, thereby maintaining the correct internal ion composition that is crucial for cell survival and function. They directly control electrical signaling in the nervous system and muscle contraction. Malfunctioning channels cause or are associated with many diseases, and a large number of drugs act directly or indirectly on channels [2].

There are many types of ion channels, each with a specialized function [3–5]. Many channels can selectively transmit or block a particular ion species and most exhibit switching properties similar to complex nanoscale electronic devices. The wide range of device-like functions exhibited by ion channels has stimulated a great deal of interest in the engineering community for their possible application in the design of novel bio-devices [6]. As integrated device features continue to shrink, statistical fluctuations and structural defects increasingly affect the reliability of solid-state nanoscale devices. Ion channels, on the other hand, have the distinct advantage of self-assembly and almost perfect structure duplication. The techniques of

*Corresponding author. Fax: +1-217-244-4333.
§Fax: +1-312-942-8711.

Molecular Simulation
ISSN 0892-7022 print/ISSN 1029-0435 online © 2005 Taylor & Francis Group Ltd
http://www.tandf.co.uk/journals
DOI: 10.1080/08927020412331308700

modern molecular biology also offer the possibility of altering protein structures with atomic resolution [7,8]. By replacing or deleting one or more of the amino acids that comprise it, the channel can be mutated, altering the distribution of charge on the protein. Engineering channels with specific conductances and selectivities is therefore conceivable. The incorporation of ion channels in the design of novel bio-devices is therefore appealing and a clear understanding of channel operation may provide a template for the design of functional elements based on synthetic molecular systems or nanotubes.

Simulations can help provide a clearer understanding of channel operation. However, the simulation of an ion channel embedded in a macroscopic membrane environment presents a formidable time and space multi-scale problem [9–13]. Channel/membrane system dimensions range from ≈ 10 to $\approx 1\,\mu$m, while specific channel functions, such as switching or selectivity, are often controlled by sub-nanometer functional sub-units of the protein. At least part of the channel system therefore needs to be represented with atomic resolution. In addition, short-range ion–ion and ion–protein interactions can be very strong so ion motion must be resolved on a femtosecond time-scale. On the other hand, ion traversal through the channel is a rare event so reliable estimates of current and other macroscopic behaviors require simulations lasting several μs. Realistic simulations are also difficult because at present the complete molecular structure is known from measurements for only a few channels. Even then, it is difficult to predict the structural and electrostatic changes that may occur when the channel is exposed to different physiological conditions.

With the broader availability of standardized software and large-scale computing power, Molecular Dynamics (MD) has become one of the most widely employed tools for studying ion dynamics in protein channels [10]. Although MD simulations can provide key information regarding the mechanisms of ion conduction in atomic detail (see Ref. [13] and references within), the computational requirements of such large-scale simulations prohibit the direct calculation of steady-state channel currents, particularly when channels are controlled by trace concentrations of ions, even on massively parallel machines. At the other end of the simulation hierarchy, continuum models based on the drift-diffusion theory used widely in the engineering community to describe charge transport in semiconductor and plasma devices [14], have been used to compute macroscopic ion current with a modest amount of computational effort [15–28]. Although drift-diffusion theory sacrifices the resolution of molecular detail, when used with an appropriate value of ion diffusivity it has been found to describe ion permeation through some channels surprisingly well. However, ion diffusivities and dielectric coefficients must be assigned with some care since the continuum paradigm deals with average densities rather than discrete particles of finite size, a premise that has been found to overestimate the ion concentration in very narrow channels [22,28]. Equilibrium Monte Carlo (EMC) simulations, in which ions are modeled as discrete particles with a finite size, but water and protein are treated as continuum dielectric media, have found recent success in explaining the selectivity mechanisms of the Ca^{++} [29–32] and Na^{+} [33] channels, indicating that competition between charge and available volume determines the channel's selectivity; however it is not clear how this approach can be used to handle ion transport in a self-consistent manner.

In order to extend simulation times beyond the current limit imposed by the computational cost of MD simulations, while still retaining some atomistic level of detail, a coarse-grained particle approach is required. In this respect, Brownian Dynamics (BD) simulations have become increasingly popular. Ion trajectories computed from the Langevin equation can be used to probe the ions' permeation pathways through the channel and statistical analysis of the trajectories yields macroscopic information regarding the channel's conductance and selectivity [26,34–43]. Although BD simulations are relatively easy to implement and yield results swiftly, representing ion–water interactions with a single friction coefficient and a random stochastic force may be an over-simplification in narrow regions of the channel where additional ion scattering mechanisms could prevail. In this paper, we describe *Bio*logy *Mo*nte *Ca*rlo (BioMOCA), an alternative three-dimensional (3D) coarse-grained particle transport model for ion channels based on the Boltzmann Transport Equation Monte Carlo (BTMC) methodology developed for semi-classical charge carrier transport in solid-state devices [44]. A brief introduction to BioMOCA has been given previously elsewhere [45], however here we furnish further details of the implementation and present a more comprehensive discussion of the various advantages and drawbacks of this approach. The interaction between ions and the surrounding channel/electrolyte environment is handled in a simplified way by treating the water, protein and lipid membrane implicitly as dielectric background media. Ion trajectories are traced in real space as sequences of free flights interrupted by thermalizing scattering events. The random duration of free flights is linked to the ion's diffusivity in the electrolyte. In contrast to electron transport in semiconductors, ions cannot be treated as point particles, since their size is comparable with the pore diameter of channels. The finite ion size is addressed here by including a pairwise Lennard-Jones potential, which prevents the unphysical coalescence of oppositely charged ions. In reality, the presence of water shells shrouding the ions plays an important role in maintaining the ions in solution, however it is not yet clear how to include this effect in the coarse-grained particle model. Electrostatic forces are calculated self-consistently from the charged particles positions by solving Poisson's equation at regular intervals. Simulation of ion transport under an applied bias across the channel is modeled in much the same way as the transport of quasiparticles is done in device simulation [44,46–49]. However, while typical semiconductor devices have highly doped contacts with fixed ion charge

and a single mobile species, the electrolyte on either side of the channel behaves more like an intrinsic semiconductor because the balance between positive and negative mobile carriers is preserved. The BioMOCA simulation code is described in detail in the following section.

Although the BTMC method has been used routinely in the semiconductor community over the past two decades, its application to ionic solutions is very recent and therefore requires validation. For this purpose, we computed the ion–ion pair correlation function $g(r)$ for several generic homogeneous electrolytes and compared them to benchmark results obtained from EMC simulations [50,51]. The function $g(r)$ plays a central role in describing the microscopic structure and thermodynamic state of a system [52–54]. For homogeneous isotropic systems, it is proportional to the probability of finding two atoms separated by a distance r. Thus, for any molecular scale simulation to be thermodynamically correct, it must reproduce the correct pair correlation function. In Third Section, we briefly review the EMC method and present the ion–ion pair correlation function calculated via these two approaches for several simple electrolytes.

Solving Poisson's equation repeatedly on a mesh that is fine enough to resolve the channel's structure and permanent charge distribution, as well as large enough to encompass the entire 3D domain, currently presents a computational bottleneck in BioMOCA simulations. In Third Section, we discuss several schemes that have been shown to significantly decrease the computational load. The pair correlation function is again used as a marker to determine that these cost-saving schemes do not alter the outcome of the simulations.

In the remaining sections, we return to the original motivation for developing BioMOCA—i.e. to simulate ion transport through protein channels embedded in lipid membranes—and present a full ion channel simulation based on gramicidin A (gA), a simple channel-forming molecule expressed by the bacterium Bacillus brevis [11,40,55–62]. The gA channel is specifically selective for small monovalent cations. Possible mechanisms underlying this selectivity have been addressed in several recent articles. In particular, it has been argued that the cancellation of the Dielectric Boundary Force (DBF) by the electrostatic forces arising from the permanent charge on the protein is responsible for the monovalent cation selectivity of gA [63,64]. We further examine the role of the distribution of permanent charge and the dielectric constant in the protein in the selectivity of gramicidin. The final section concludes with a discussion of this work, as well as some of the aspects of the coarse-grained approach that require further work in the future.

2. The BioMOCA–Boltzmann Transport Monte Carlo Code

BioMOCA is a 3D code for simulating ion transport in electrolyte environments surrounding proteins, based on the Boltzmann Transport Monte-Carlo (BTMC) [44] and particle–particle–particle-mesh (P^3M) methodologies [46]. Although specifically designed to simulate transport through ion channel proteins embedded in membranes, BioMOCA can also be used to study ion transport in other proteinaceous environments as well as bulk electrolyte solutions. In order to reduce the amount of computation, the protein, membrane and water are all treated as dielectric background media. Ion motion is assumed to be classical and overdamped by frequent scattering events with water molecules. In between scattering events, the ions move according to Newton's laws of motion in response to the local field. Trajectories are synchronously propagated in time and space by integrating the equations of motion using the second-order accurate leap-frog scheme [46]. Ion positions r and forces F are defined at time-steps t, $t + \mathrm{d}t$ while ion velocities are defined at $t - (\mathrm{d}t/2)$, $t + (\mathrm{d}t/2)$. The finite difference form of the equations of motion is thus,

$$\begin{aligned} \underset{\sim}{v}^{t+\frac{\mathrm{d}t}{2}} &= \underset{\sim}{v}^{t-\frac{\mathrm{d}t}{2}} + \underset{\sim}{F}^{t}_{\mathrm{tot}}\,\mathrm{d}t \\ \underset{\sim}{r}^{t+\mathrm{d}t} &= \underset{\sim}{r}^{t-\mathrm{d}t} + \underset{\sim}{v}^{t+\frac{\mathrm{d}t}{2}}\,\mathrm{d}t \end{aligned} \tag{1}$$

where the total force on the ion $\underset{\sim}{F}_{\mathrm{tot}}$, is the sum of the electrostatic component and a pairwise ion–ion interaction component which represents the finite size of the ions. The overall flow of control in the BioMOCA algorithm is illustrated in figure 1 and the various steps are described in detail below.

2.1 Field solution

The local electrostatic potential $\phi(\underset{\sim}{r})$ is obtained self-consistently by solving Poisson's equation,

$$\nabla \cdot \left(\varepsilon(\underset{\sim}{r})\nabla\phi(\underset{\sim}{r})\right) = -\left(\rho(\underset{\sim}{r})_{\mathrm{ions}} + \rho(\underset{\sim}{r})_{\mathrm{perm}}\right) \tag{2}$$

where $\rho_{\mathrm{ions}}(\underset{\sim}{r})$ and $\rho_{\mathrm{perm}}(\underset{\sim}{r})$ are respectively, the densities of mobile ions and permanent fixed charge on the protein, and $\varepsilon(\underset{\sim}{r})$ is the local dielectric constant. Solving equation (2) over the entire domain subject to specific Dirichlet boundary conditions provides a simple way to include an applied bias and the effects of image charges induced at dielectric boundaries. The mobile charge density $\rho_{\mathrm{ions}}(\underset{\sim}{r})$ is recomputed at regular intervals from the current positions of all ions in the system. Each ion's

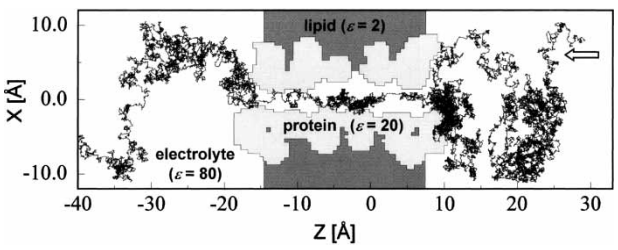

Figure 1. Flowchart of the BioMOCA algorithm.

charge is associated to a finite rectilinear grid using the cloud-in-cell (CIC) scheme [46] to weight the charge to the eight nearest grid points. Equation (2) is then discretized using finite differences or finite elements and solved using either conjugate gradient [65] or multi-grid [66] methods, subject to boundary conditions chosen to suit the particular system being modeled. The electrostatic field $\underset{\sim}{E}_{\text{mesh}}$ at each grid point is obtained from the potential using second-order finite differences and the field at the eight nearest grid points is then weighted back to the ion using the same interpolation kernel that was used to map the charge density. The grid spacing is typically 1 Å.

The discretization of Poisson's equation leads to an unavoidable truncation of the short-range component of the electrostatic force, which can be corrected using the P^3M scheme. Short-range charge–charge electrostatic interactions are included explicitly by evaluating the Coulomb field $\underset{\sim}{E}^{\text{coul}}$ in a finite short-range domain Ω^{sr} surrounding each ion. The total electrostatic field $\underset{\sim}{E}^{\text{tot}}$ is obtained by adding the short-range Coulomb component (particle–particle) $\underset{\sim}{E}^{\text{coul}}$ with the field obtained from Poisson's equation (particle-mesh) $\underset{\sim}{E}^{\text{mesh}}$, plus a correction or reference term $\underset{\sim}{E}^{\text{ref}}$ to avoid double counting in the overlap region between the short-range and global domains. Thus the total field acting on ion i is written as

$$\underset{\sim}{E}_i^{\text{tot}} = \underset{\sim}{E}_i^{\text{mesh}} + \sum_{\substack{i \neq j \\ r_j \in \Omega_i^{\text{sr}}}} \underset{\sim}{E}_{ij}^{\text{coul}} - \underset{\sim}{E}_{ij}^{\text{ref}} \tag{3}$$

where $\underset{\sim}{E}_i^{\text{mesh}}$ is the field acting on ion i, obtained from Poisson's equation, $\underset{\sim}{E}_{ij}^{\text{coul}}$ is the Coulomb field acting on ion i due to all ions j that lie within the short-range domain Ω_i^{sr} surrounding ion i, and $\underset{\sim}{E}_{ij}^{\text{ref}}$ is the reference term that removes the contribution to $\underset{\sim}{E}_i^{\text{mesh}}$ from ions j that lie within Ω_i^{sr}. Ideally $\underset{\sim}{E}_{ij}^{\text{ref}}$ should cancel the mesh component inside the short-range domain while outside the short-range domain it should cancel the Coulomb component. In practice there is no computationally reasonable procedure for determining the exact reference term. Hockney and Eastwood describe an approximation that minimizes the error in transitioning from the global to short-range domains, by effectively ascribing a finite size to the charged particle [46]. Here we use a simpler and less computationally burdensome approach, approximating the short-range component of the mesh force using the analytical expression for the Coulomb field due to a charged sphere of radius $r_a \simeq 1.5\Delta$ where Δ is the uniform mesh spacing. The charge distribution that best represents the short-range behavior of the mesh force is one that is linearly decreasing with radius, *viz.*

$$\rho(r) = \frac{3q}{r_a^2}\left(1 - \frac{r}{r_a}\right) \qquad r \leq r_a. \tag{4}$$

Using equation (4), the reference term is given by

$$\underset{\sim}{E}_{ij}^{\text{ref}} = \begin{cases} \frac{3q_j}{\pi\varepsilon r_{\text{sr}}^2}\left(\frac{s}{3r_{\text{sr}}} - \frac{s^2}{4r_{\text{sr}}^2}\right)\frac{\underset{\sim}{r}_i - \underset{\sim}{r}_j}{s} & \underset{\sim}{r}_j \in \Omega_i^{\text{sr}} \\ \frac{q_j}{4\pi\varepsilon}\frac{\underset{\sim}{r}_i - \underset{\sim}{r}_j}{s^3} & \underset{\sim}{r}_j \notin \Omega_i^{\text{sr}} \end{cases} \tag{5}$$

where $\underset{\sim}{r}_i$ and $\underset{\sim}{r}_j$ are the locations of ions i and j, Ω_i^{sr} is sphere of radius $r_{\text{sr}} = r_a$ centered on $\underset{\sim}{r}_i$ and $s = |\underset{\sim}{r}_i - \underset{\sim}{r}_j|$ is the separation between ions i and j. In practice $\underset{\sim}{E}_{ij}^{\text{ref}}$ is only ever computed for those ions that reside within the short-range domain since the last two terms of equation (3) cancel exactly for ions located outside Ω_i^{sr}. Extensive benchmarking discussed in the following section has demonstrated that this approximation works well for ionic solutions. This treatment of the electric field is quite different from that in traditional protein molecular dynamics [9]. There periodic boundary conditions are almost invariably used, and when particle-mesh methods are used, they are used quite differently.

2.2 Dielectric coefficient

An important aspect for ion channel simulations that compute electrostatic forces from Poisson's equation is the assignment of appropriate values for the dielectric coefficient of the protein and membrane. The dielectric coefficient determines the strength of the interaction between two charged species as well as the self-force felt by an ion as it approaches a boundary between two regions having different dielectric coefficients, hereafter referred to as the DBF. The resulting potential energy barrier faced by a single point charge trying to pass through the center of the channel is strongly dependent on the relative values of the dielectric coefficient in the two regions; as we show later, reducing the dielectric coefficient in the protein from $\varepsilon_{\text{p}} = 20$ to $\varepsilon_{\text{p}} = 2$ increases the height of the barrier by almost a factor of three, which has strong implications for the channel's conductance. It is therefore crucial to have a realistic idea of the dielectric properties of the channel before drawing any conclusions about channel conductance from simulations.

The task of assigning specific values for the dielectric coefficient in the protein and membrane environments is problematic because the protein environment can respond to an external field in several different ways. For example, field-induced dipoles, re-orientation of permanent dipoles and larger scale re-organization of ionized side-chains and water molecules, both within the interior and on the surface of the protein, all contribute to the protein's dielectric response on different relaxation time-scales. When deciding what value to assign to protein dielectric coefficient ε_{p} one must first consider how much physics is included explicitly in the model. In MD simulations where all of the charges and dipoles are included explicitly, then clearly ε_{p} should be equal to 1 everywhere.

For models that treat only the field-induced atomic polarization of the proteinaceous region implicitly, it has

been suggested that $\varepsilon_p \approx 2$ is more appropriate. However, when protein and water re-organization are also treated implicitly, as is the case in BioMOCA and most other coarse-grained particle ion channel simulation codes, the dielectric coefficient is hard to define, particularly when ion motion takes place on the same time-scale as the protein's response to its presence. It has been suggested that for continuum models that seek to encapsulate the dielectric response of the water and protein side-chains with a single dielectric coefficient, the value of ε_p should be greater than 2 [67]. The issue of protein dielectric coefficients is addressed in detail in several recent articles (see Refs. [67–70] and references within).

In addition to the protein and membrane dielectric coefficients, some thought must be given to assigning values for the dielectric coefficients of the aqueous regions of the ion channel system. The electrolyte bath regions are generally given the same dielectric coefficient as bulk water, *viz.* $\varepsilon_w \simeq 80$. However, in most ion channels the pore is very narrow and is often lined with highly charged residues and/or strong permanent dipoles that can form hydrogen bonds with water molecules within the channel. As a result, water molecules can be highly ordered within the channel pore, restricting their response to external fields [13,71]. In the case of the gramicidin channel, which is discussed later in this paper, correlated motion of water molecules inside the channel is extreme. The pore is lined with strongly polarized carbonyls and NH bonds in the polypeptide backbone, which hydrogen-bond to each other, helping to stabilize the channel's helical structure. These dipoles are tilted with respected to the channel axis such that the carbonyls protrude slightly into the pore forming hydrogen bonds with water molecules which, due to the narrow width of the pore, must traverse the channel in single file [72]. As a result, water is extremely ordered within the channel and the dielectric coefficient ε_{ch} can be expected to be significantly lower than the value used for water under bulk conditions, and more than likely anisotropic. Computing electrostatic forces acting on ions in regions surrounding a sharp transition in dielectric coefficient poses additional numerical complications. Ideally the dielectric coefficient should decrease gradually from the bulk-like bath regions to the channel pore. This aspect of the BioMOCA simulator is still under development. For the simulations presented here we have adopted the same approach as several other groups [17,18,21,22,24–46] and use $\varepsilon_{ch} = 80$ inside the channel pore.

With these considerations in mind, BioMOCA is designed to handle any user-provided distribution of dielectric coefficient. For the results presented here we have chosen to specify ϵ on a region by region basis. However, the code is flexible enough to accept a grid-based description of dielectric coefficient. The technique used to define the boundaries between the various regions is discussed later in this section.

2.3 Ion size

In addition to electrostatic forces acting on the ions, a pairwise repulsive force is also included to mimic ionic core repulsion, thus preventing ions from overlapping or coalescing unphysically. Several forms for the interaction potential are reported in the literature, all requiring fitting parameters. The most commonly employed is the Lennard-Jones 6–12 potential, which does an admirable job of predicting the properties of condensed noble gases. For ionic systems another simple inverse power law where the value of the index parameterizes the hardness of the ionic core repulsion is often used. Unlike the Lennard-Jones potential this potential ignores the effects of field-induced polarization. For the results presented in this paper we have used a truncated-shifted form of the Lennard-Jones potential, discussed further in the following section. However, in principle any analytic form can be used. The issue of how to calibrate these interaction potentials and fitting parameters, though a most important one, is not addressed in this paper. It is a constant issue of discussion among us, because the properties of concentrated salt solutions depend so sensitively on the diameter of their ions [73–76].

2.4 Ion–water interaction

Unlike MD simulations, which treat all particle–particle interactions explicitly, BioMOCA simulations replace the individual water molecules with a continuum background media and ion–water interactions are handled using the BTMC method. Ion trajectories are randomly interrupted by scattering events that account for the ions' diffusive motion in water. The flight times T_f between these scattering events or collisions are generated statistically from the total scattering rate for all collision mechanisms $\lambda_{tot}(\vec{p}(t))$ according to

$$-\ln r = \int_0^{T_f} \lambda_{tot}\big(\vec{p}(t)\big)\mathrm{d}t \tag{6}$$

where r is a random number uniformly distributed on the unit interval. In general the scattering rate can depend on particle momentum $\vec{p}$, which in turn will depend on the ion's local environment, and should constitute the sum of individual scattering rates for various scattering processes. At the start of each ion trajectory a random number r is used to set the flight counter α_0, given by the left-hand side of equation (6) which can be rewritten as

$$\alpha_0 = -\ln r = \sum_{i=0}^{n-1} \int_{i\mathrm{d}t}^{(i+1)\mathrm{d}t} \lambda_{tot}(\vec{p}(t))\mathrm{d}t + \int_{n\mathrm{d}t}^{T_f} \lambda_{tot}(\vec{p}(t))\mathrm{d}t$$

$$= \sum_{i=0}^{n-1} \Gamma_i\,\mathrm{d}t + \Gamma_n T_f \tag{7}$$

where Γ_i is the maximum scattering rate during the ith time-step. At the beginning of each time-step, the flight counter is incremented by an amount $\alpha_{i+1} = \alpha_i + \Gamma_i \mathrm{d}t$. As long as $\alpha_{i+1} > 0$, the ion trajectory is integrated over the whole time-step. When $\alpha_{i+1} < 0$, the ion is assumed to have scattered with a water molecule during the time interval $(t_i, t_i + \mathrm{d}t)$. The trajectory is integrated up to the time of scattering over the sub-time-step $(t_i, t_i + \mathrm{d}t')$, where $\mathrm{d}t' = T_\mathrm{f} - t_i$ is given by α_i/Γ_i. Another random number is then used to select which type of scattering event took place and the final state of the ion is selected according to the particular scattering model implemented. Although BioMOCA is equipped to handle multiple scattering processes, and space and momentum dependent scattering rates, for this work we have assumed a single scattering mechanism that "thermalizes" the ion, with a constant scattering rate for each species, linked to the ion's diffusion coefficient in water. That is to say, the final state is selected randomly from a Maxwellian distribution, the flight counter is reset using another random number and the ion trajectory is integrated over the remainder of the time-step. We note that in simulations of regions of restricted volume, such as inside the channel pore, additional scattering mechanisms may alter the scattering rate significantly. Scattering models that include position-dependent diffusion coefficients obtained from MD simulations will be addressed elsewhere.

2.5 Ion–protein interaction

In order to model the interaction of ions with the protein and membrane, the boundary between electrolyte, protein and lipid membrane regions must first be defined. Due to the lack of structural information, as well as tools for representing molecular structure within the simulation framework, early coarse-grained particle ion channel simulations often used simple geometric structures (e.g. cylindrical holes and toroids) to represent the protein boundary as a smooth surface [34–36,41,42]. The simulation domain was thus divided into regions that ions can physically access and regions from which they are excluded. Although this approach is simple to implement, it does not capture the detailed protein topography, which can play an important role in the channel's function.

Despite the difficulty in crystallizing ion channel proteins, high-resolution X-ray crystallographic measurements of complete molecular structures have recently been obtained for several ion channels [13,77].‡ These molecular structures provide information about the type and location of the atoms that form the protein, although they of course do not settle the location or description of dielectric boundaries, or distributions of permanent charge of the channel protein. In addition, several force-fields are available in the literature providing information about the charge and radii of the atoms in different amino-acid groups. These force fields are the result of an extraordinary effort to choose atomic parameters that reproduce important *macroscopic* properties of amino acids and proteins [9]. There is not agreement, however, about which macroscopic properties are important, e.g. solvation energy or/and activity coefficient, nor are the choices used historically to design each force field always apparent. Clearly, the force fields are macroscopic fitting parameters subject to ambiguity and error as other macroscopic parameters (e.g. dielectric coefficient), and future work will be needed to optimize their choice. The molecular structures together with the force-fields provide the coordinates, charge and radii of each constituent atom of the protein. One way to model the interaction between ions and protein surface is to use a radially symmetric interaction potential (e.g. Lennard Jones) for each near-surface protein atom, of which the short-range repulsive component "naturally" prevents the ions from penetrating the protein. Molecular dynamics simulations of the protein equilibrated *in situ* in a lipid bilayer can also provide structural information for the membrane, allowing the membrane surface to be similarly modeled. However this approach can be computationally costly, especially for larger protein channels like porins. Furthermore, this approach assumes the protein to be a static structure, ignoring the movement of the protein in response to applied fields and thermal fluctuations.

In BioMOCA, we take a simpler approach that partitions the simulation domain into contiguous regions. Many open-source molecular biology packages now have built-in facilities that determine the regions accessible to finite-sized ions in a protein system mapped onto a rectilinear grid. We have incorporated the scheme implemented in the Adaptive Poisson Boltzmann Solver (APBS) [66] into the BioMOCA simulator. The algorithm takes as input the molecular structure of a given protein channel, which is publicly available in the Protein Data Bank,‡ along with one of the force-fields (atomic radii and partial charges) described earlier. A uniform rectilinear grid is placed over the domain and a ball having radius appropriate to a water molecule is used to sample the 3D space. Grid points that cannot be accessed without the ball overlapping protein are labeled as protein and the rest are considered electrolyte. The volume embedding the protein in the direction radial to the channel axis is then designated as lipid membrane, to create three contiguous regions (protein, lipid, and channel) connecting two electrolyte baths. The regions classified as protein and lipid are deemed inaccessible to ions. The ions themselves are assigned a finite radius, equal to the Pauling ionic radius [3]. If any point within the sphere thus defining the ion crosses the protein or membrane boundary during a time-step, the ion is assumed to have collided or interacted in some way with the protein/membrane. The ion is returned to its position at the beginning of the time-step and reflected diffusively. This process is repeated until the ion's

‡http://www.rcsb.org/pdb/

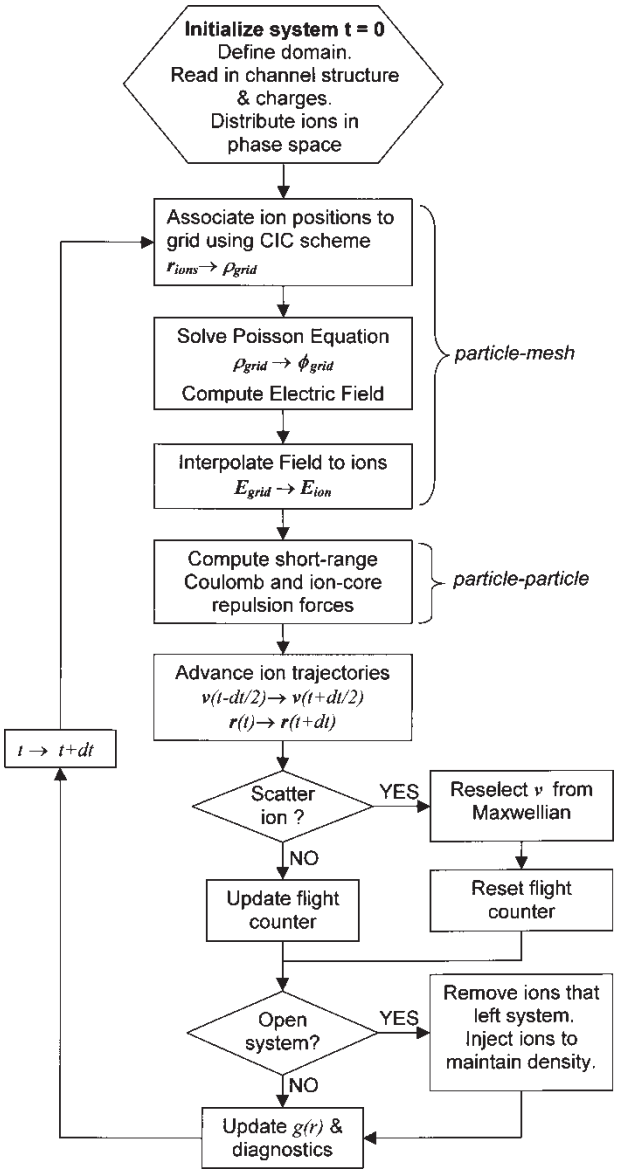

Figure 2. A 2D slice through the 3D BioMOCA domain, passing through the center of the gramicidin ion channel *in situ* in a dielectric slab representing the lipid membrane. A single Na^+ ion trajectory that passed through the channel is superimposed.

final position lies outside the protein/membrane region. A 2D slice through the 3D BioMOCA representation of the gramicidin ion channel *in situ* in a neutral lipid membrane of thickness 22 Å, is shown in figure 2. Planar contacts are included at either end of the domain to enable a fixed bias voltage to be applied across the system. The trajectory of a single Na^+ ion that successfully passed through the channel during a typical simulation is also shown.

2.6 Boundary conditions

Experimentally, the electrical and physiological properties of a single ion channel can be measured by inserting the channel into a lipid bilayer (membrane) separating two baths containing solutions of specific concentrations [78]. Electrodes are immersed in the baths to maintain a constant bias voltage across the membrane. Formulating boundary conditions that adequately represent these contact regions can require extremely large baths and is a challenging task. For general BioMOCA applications, we assume that beyond a Debye length from the membrane the average electrostatic potential and ion densities do not vary appreciably, an assumption supported by the results of recent continuum simulations [25]. For salt concentrations considered here, this distance is of the order of 10 Å. We therefore impose Dirichlet boundary conditions on the potential at the two domain boundary planes that lie parallel to the membrane, taking care to ensure that the Dirichlet boundary planes are sufficiently far from the membrane. Homogeneous (i.e. zero) Neumann boundary conditions are imposed at all other domain boundaries. Periodic boundary conditions are never used.

To model electrolyte baths of fixed concentration on either side of the membrane, a constant ion population is maintained in buffer regions that extend into the domain from the Dirichlet boundary planes. Ions that leave the domain through the Dirichlet boundary planes are removed from the simulation. At the end of each time-step the total number of ions of each species in the buffer regions is counted. If the ion population falls below the value representing the desired density new ions are injected with a Maxwellian velocity to maintain the given density. It should be noted however, that ions are never artificially removed from these buffer regions. Ions that attempt to cross the Neumann boundary planes are reflected elastically.

3. Validating BioMOCA for simulation of electrolytes

The BTMC method is a numerically efficient way to solve the Boltzmann Equation for semi-classical transport. It has been used to study charge transport in electron devices for over four decades [44,46–49]; however, its application to ion transport in electrolytes is new. Several other groups have developed 3D coarse-grained particle based codes for simulating transport in ion channels [26,34–43,79]. Unlike BioMOCA however, these codes use Brownian Dynamics to describe ion transport. The key advantage that the transport Monte-Carlo approach holds over Brownian Dynamics is the flexibility to use different ion–water scattering models in different regions of the channel environment. In the limit of high friction both approaches should give the same result. The most conspicuous difference between the charge carriers in semiconductor devices and those of electrolytes is the physical size of the charge. Unlike electrons, the size of the ions cannot be ignored in ion channels systems, since the dimensions of the channel pore are often comparable to that of the ions. Before embarking on a full-scale ion channel simulation, it is important to first check that both the P^3M scheme and the ion–ion interaction are implemented correctly in BioMOCA. For this purpose we have benchmarked

BioMOCA against the well-established EMC simulation method by comparing the ion–ion pair correlation functions $g(r)$ for several model electrolytes under equilibrium conditions computed using both approaches. The EMC method has been widely used to describe the properties of ensembles of hard spheres and is described below and in further detail in Refs. [29,80].

The pair correlation function provides a quantitative description of the microscopic structure of matter and can be used to derive macroscopic thermodynamic properties of the system, such as pressure and density [52–54]. It is therefore seen as a suitable first measure to validate the BMTC methodology for electrolytes. The pair correlation function $g(r)$ is defined as

$$g(r) = \frac{V}{N^2}\left\langle \sum_i \sum_{j \neq i} \delta(r - r_{ij}) \right\rangle \tag{8}$$

where $V_s = L \times L \times L$ is the system volume, N_s is the number of particles, r_{ij} is the distance between particles i and j, and the angular brackets denote a time average. Since both EMC and BMTC simulation methods provide particle coordinates in real space, $g(r)$ is readily computed by simply counting the number of particles $N_k(r, \Delta r)$ found in a spherical shell of radius r and thickness Δr, centered at each particle,

$$g(r) = \frac{\frac{1}{M}\sum_{k=1} N_k(r, \Delta r)}{\frac{N_s^2}{2V_s} V(r, \Delta r)} \tag{9}$$

where the time average is performed explicitly over M time-steps.

We now consider three generic electrolytes under bulk equilibrium conditions, consisting of two ionic species that interact via the Coulomb potential and an additional ion–ion pairwise Lennard-Jones 6–12 potential. The latter represents the ionic core repulsion that prevents ions from overlapping or coalescing which would clearly be unphysical. The Lennard-Jones interaction is modified to retain only the short-range repulsive component, as described by Equation (10), and illustrated in figure 3

$$U_{LJ}(r_{ij}) = \begin{cases} 4\varepsilon_{LJ}\left(\left(\frac{\sigma_{ij}}{r_{ij}}\right)^{12} - \left(\frac{\sigma_{ij}}{r_{ij}}\right)^{6}\right) + \varepsilon_{LJ} & r_{ij} < 2^{1/6}\sigma_{ij} \\ 0 & r_{ij} > 2^{1/6}\sigma_{ij} \end{cases} \tag{10}$$

where ε_{LJ} is the Lennard-Jones energy parameter and $\sigma_{ij} = (\sigma_i + \sigma_j)/2$ is the average of the individual Lennard-Jones distance parameters for particles i and j. For the results presented here we set $\varepsilon_{LJ} = k_B T$ and $T = 298.15$ K.

EMC simulations involve sampling the phase space of a system in thermodynamic equilibrium. For the EMC results presented here, the canonical (NVT) ensemble was used. Particles are distributed randomly in the phase space of a fixed volume and periodic boundary conditions are imposed to mimic bulk conditions. The pair correlation function is computed by attempting to alter the system configuration. Each EMC step involves displacing a single ion randomly in the simulation volume. The change is accepted with probability $\exp(-\Delta U/k_B T)$ where ΔU is the energy cost of the change, determined from the Coulomb and Lennard-Jones interaction potentials. The long-range component of the Coulomb interaction was determined in Fourier Space using an Ewald sum and the Lennard-Jones interaction was determined directly in real space. Water was treated as a dielectric continuum using a permittivity $\varepsilon_w = 80$. Each EMC simulation was run long enough to yield a relatively smooth function $g(r)$, sampled at every iteration in discrete bins of width $h = 0.3$ Å. CPU requirements on a single processor SGI Origin2000 (250 MHz R10k) were of the order of a few hours.

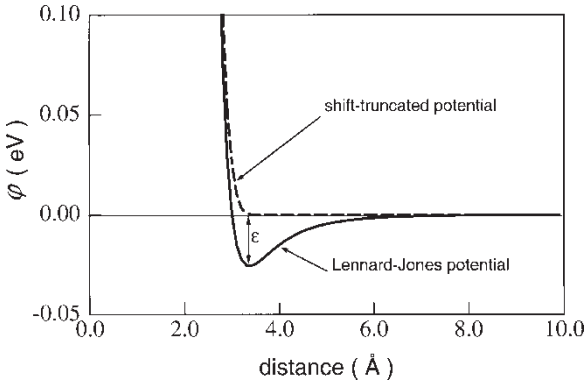

Figure 3. Magnified view of the ion–ion pairwise Lennard-Jones 6–12 potential, shifted and truncated to include only the short-range repulsive component which prevents ions from coalescing.

We consider first a simple monovalent electrolyte of two oppositely charged ion species having $\sigma_+ = \sigma_- = 3$ Å, at a concentration of 1 M. Ion–water scattering rates were chosen based on the masses of Na^+ and Cl^- ions, and the diffusion coefficients of Na^+ in bulk water [81], yielding $\lambda_+ = 8.13 \times 10^{13}\, s^{-1}$ and $\lambda_- = 5.27 \times 10^{13}\, s^{-1}$. In order to model bulk-like conditions using BioMOCA, we consider a closed system (i.e. ions are reflected off all domain boundaries) sufficiently large to minimize edge effects associated with the finite domain and mixed Dirichlet/Neumann boundary conditions. To avoid skewing of the pair correlation function by the finite domain used in BioMOCA, 26 replica domains are placed directly adjacent to the primary domain. Of the 27 particles (original particle plus 26 replicas) only the one that lies within a distance $L/2$ of the center of the shell is counted in Eq. (9). The domain thus consists of a cube of side-length $L = 192$ Å, discretized into $48 \times 48 \times 48$ cells, with mesh spacing $\Delta = 4$ Å. For a monovalent solution at a concentration of 1 M these domain dimensions yield a total ion population of 8524. By contrast, since the EMC simulations employ periodic boundary conditions, edge effects are not problematic, thus permitting the use of smaller domains ($L = 69.251$ Å) and hence a much smaller ion population of only 400.

Cation–cation $g_{++}(r)$, anion–anion $g_{--}(r)$ and cation–anion $g_{+-}(r)$ pair correlation functions computed for

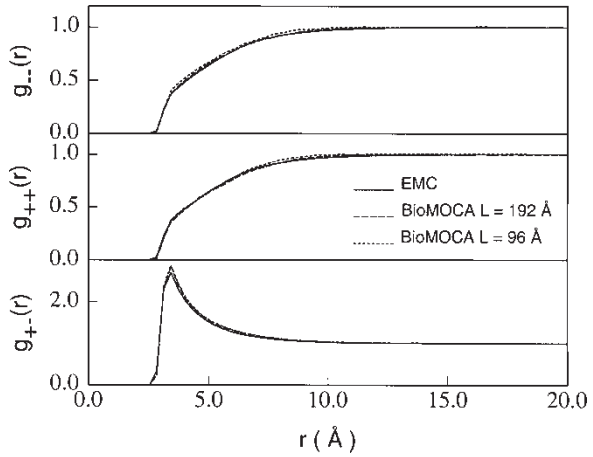

Figure 4. $g_{--}(r)$, $g_{++}(r)$ and $g_{+-}(r)$ pair correlation functions computed from EMC and BioMOCA simulations for a 1 M solution of a simple monovalent electrolyte consisting of two oppositely charge ion species of equal size $\sigma_+ = \sigma_- = 3$ Å. Solid lines indicate EMC results. BioMOCA results computed using (i) $L = 192$ Å, $48 \times 48 \times 48$ cells, $\Delta = 4$ Å are shown by dashed lines and (ii) $L = 96$ Å, $24 \times 24 \times 24$ cells, $\Delta = 4$ Å by dotted lines.

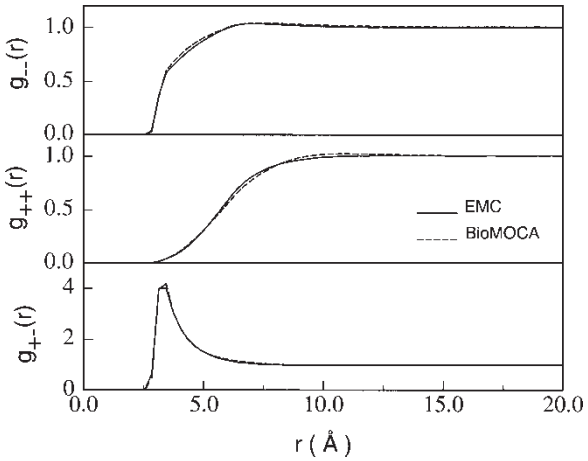

Figure 5. $g_{--}(r)$, $g_{++}(r)$ and $g_{+-}(r)$ pair correlation functions computed from EMC (solid lines) and BioMOCA (dashed lines) simulations for a 1 M solution of a divalent electrolyte consisting of two equally sized ion species described by: $\sigma_+ = \sigma_- = 3.0$ Å, $z_+ = +2$, $z_- = -1$.

the system described above are shown in figure 4. The dashed line indicates BioMOCA results while the solid line shows EMC results. The comparison between the two different approaches is excellent. For this result the BioMOCA simulation was run for 2.1 ns, using an ion integration time-step of 10 fs. After a 100 ps equilibrating period the pair correlation functions were sampled every 1 ps, into discrete bins of width $h = 0.3$ Å. Long-range electrostatic fields, obtained from the solution of Poisson's equation (Particle-Mesh), were updated every 10 time-steps (100 fs) while the short-range component (Particle–Particle) was updated every time-step. The CPU requirements for these parameters amount to roughly 22 h on an Intel 2.4 GHz processor. Using a smaller domain can drastically reduce the run-times; however, as mentioned above, since BioMOCA does not use periodic boundary conditions, the smaller the domain size the more the system departs from bulk-like conditions. To see this effect we halved the side-length of the box while keeping the mesh spacing the same, thereby reducing the number of grid points and ion population by a factor of 8, and performed the same simulation. Although the run-time is now reduced to ≈80 min, the pair correlation functions, also shown in figure 4 by the dotted line, are slightly degraded.

Figures 5 and 6 show the pair correlation functions computed on domain of side-length $L = 192$ Å, discretized into $48 \times 48 \times 48$ cells, with mesh spacing $\Delta = 4$ Å for 1 M solutions of (i) a divalent electrolyte described by: $\sigma_+ = \sigma_- = 3.0$ Å, $z_+ = +2$, $z_- = -1$ (figure 5) and (ii) a monovalent electrolyte of dissimilar ion sizes, described by: $\sigma_+ = 1.9$ Å, $\sigma_- = 3.62$ Å, $z_+ = +1$, $z_- = -1$ (figure 6). All other simulation parameters including scattering rate remain the same as above. The agreement with EMC simulations is again excellent, lending confidence in the ability of BioMOCA to handle multivalent solutions of different ionic species.

3.1 Computational issues

Repeatedly solving Poisson's equation in real space currently presents the main computational bottleneck in the BioMOCA simulations. For the $48 \times 48 \times 48$ grid used in figure 4, roughly 32% of the total CPU is consumed by the solution of Poisson's equation. However, with such a large domain ($L = 192$ Å) the number of ions is so great (≈8500) that the magnitude of this bottleneck is somewhat masked by other tasks that scale with the number of particles, e.g. integrating trajectories (≈26%) and computing short-range forces (≈27%). In actual BioMOCA ion channel simulations the number of ions is typically less than 100 and the fraction of time spent solving Poisson's equation can be as much as 85%. Since the CPU cost of the Poisson solution scales almost linearly with the total number of grid points, there is clear motivation to use the coarsest possible mesh. In this

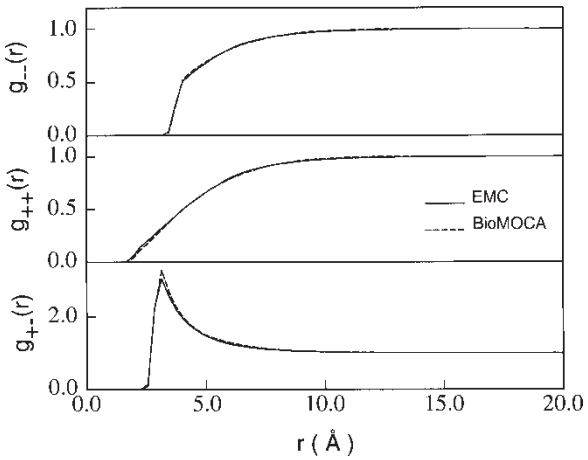

Figure 6. $g_{--}(r)$, $g_{++}(r)$ and $g_{+-}(r)$ pair correlation functions computed from EMC (solid lines) and BioMOCA (dashed lines) simulations for a 1 M solution of a monovalent electrolyte of dissimilar sized ions described by $\sigma_+ = 1.9$ Å, $\sigma_- = 3.62$ Å.

section, we illustrate this issue by returning to the 1 M monovalent solution consisting of two equally sized ion species ($\sigma_+ = \sigma_- = 3$ Å), and re-computing the pair correlation functions on a smaller cubic domain of side-length $L = 96$ Å, using the following progressively coarser meshes: (1) $48 \times 48 \times 48$: $\Delta = 2$ Å, (2) $24 \times 24 \times 24$: $\Delta = 4$ Å, (3) $12 \times 12 \times 12$: $\Delta = 8$ Å, (4) $6 \times 6 \times 6$: $\Delta = 16$ Å and (5) $3 \times 3 \times 3$: $\Delta = 32$ Å. For the three finest meshes ($\Delta = 2$ Å, $\Delta = 4$ Å and $\Delta = 8$ Å), the pair correlation functions were computed both with (P^3M) and without (PM) the correction for the truncation of the short-range component by the mesh.

Agreement between the pair correlation functions computed with P^3M scheme was excellent across the first four mesh configurations ($\Delta = 2$ Å, $\Delta = 4$ Å, $\Delta = 8$ Å and $\Delta = 16$ Å), with some distortion observed on the coarsest mesh ($\Delta = 32$ Å) where, due to the grid points being so few, the application of mixed Dirichlet/Neumann boundary conditions starts to perturb both the global solution of Poisson's equation and the local correction term $\underline{E}^{\text{ref}}$, creating non-bulk-like conditions. Due to space restrictions we do not show these results. Figure 7, however, compares the pair correlation functions computed with only the PM scheme against a base case computed with the P^3M scheme on the $\Delta = 2$ Å mesh. The corresponding run-times for each 2.1 ns simulation are plotted in figure 8. Open symbols indicating results obtained using the PM scheme and closed symbols indicating those obtained with the P^3M scheme.

Firstly, comparing run-times for the two simulations (PM vs. P^3M) performed on the finest grid ($\Delta = 2$ Å) demonstrates that the P^3M scheme adds little if any computational overhead, a result that is hardly surprising, since the short-range correction term is rarely invoked when the mesh spacing is smaller than the ion diameter ($\Delta < \sigma_{LJ}$). The strong short-range repulsive interaction in equation (10) ensures that the event of two ions occupying

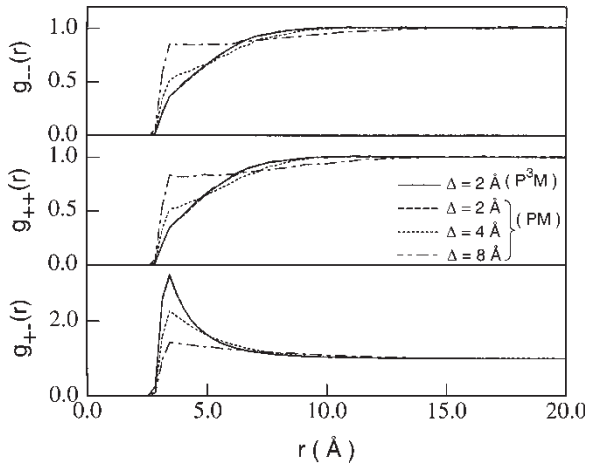

Figure 7. $g_{--}(r)$, $g_{++}(r)$ and $g_{+-}(r)$ pair correlation functions for a 1 M monovalent electrolyte described by $\sigma_+ = \sigma_- = 3.0$ Å computed from BioMOCA using the PM scheme on progressively coarser meshes: $\Delta = 2$ Å, $\Delta = 4$ Å and $\Delta = 8$ Å, compared to the base case computed on a $\Delta = 2$ Å mesh using the P^3M scheme.

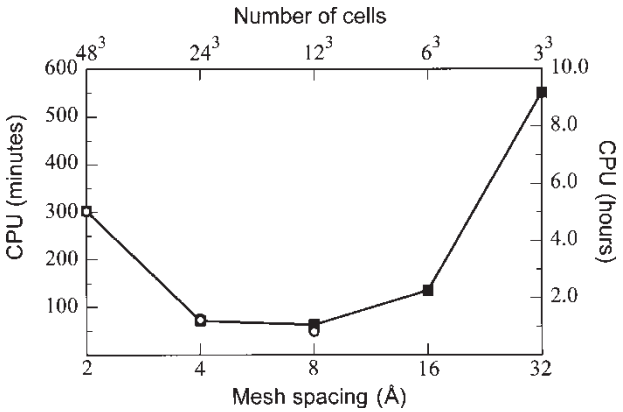

Figure 8. CPU time as a function of mesh spacing for the pair correlation function calculations in figure 7.

the same or neighboring mesh cells at the same time is extremely unlikely. Therefore, truncation of short-range electrostatic forces by the mesh, which only becomes critical at inter-particle distances $r \simeq 1.5\Delta$, is not problematic and, as shown in figure 7, the pair correlation functions computed on the $\Delta = 2$ Å grid with the P^3M scheme (solid line) and with the PM scheme (dashed line) are indistinguishable. If ions are present at high concentrations, say greater than 1 M, one might expect greater sensitivity to the estimation of short range electrostatic forces.

When the mesh spacing is doubled from $\Delta = 2$ Å to $\Delta = 4$ Å, the run-time is reduced 5-fold. However, as figure 7 shows, the truncation of the short-range Coulomb forces by the mesh is now apparent in the pair correlation functions computed using only the PM scheme (dotted line), which are noticeably distorted. The correct pair correlation function was effectively recovered with negligible overhead using the P^3M scheme. The dramatic speed-up observed when the grid spacing is increased from $\Delta = 2$ Å and $\Delta = 4$ Å saturates at $\Delta = 8$ Å because the work involved with computing the pair correlation function and the particle transport now dominates the computational load. The force truncation is clearly unacceptable as evidenced by the severe distortion of the pair correlation function. The increase in $g_{++}(r)$ and $g_{--}(r)$, and decrease in $g_{+-}(r)$ at short interaction distances ($r = 3$ Å to $r = 6$ Å) indicates that the electrostatic interaction is grossly underestimated by the particle-mesh scheme. Again, the original pair correlation functions were recovered by using the P^3M scheme, albeit with some computational overhead, which increases dramatically with further increases in mesh spacing. As the mesh becomes coarser the size of the short-range domain ($r_a \simeq 1.5\Delta$), and hence the number of particles residing therein, also increases. As a result the overhead of directly computing the short-range Coulomb forces far outweighs any speed-up up obtained from reducing the number of grid points, as clearly illustrated by the CPU time required for the extreme case of $\Delta = 32$ Å.

3.2 Relaxing the frequency of Poisson updates

In addition to reducing the number of grid points, substantial reduction in the computational load can be achieved by relaxing the time interval between successive solutions for the electrostatic field. Ion transport in electrolyte is highly collisional and under bulk equilibrium conditions ion transport is largely diffusive [3]. The ion root-mean-square displacement scales with time as $x_{\mathrm{rms}>} = (6Dt)^{1/2}$, where D is the diffusion coefficient [82]. Over a time scale of 1 ps the ion diffusion length in a typical bulk electrolyte is about 1 Å. Therefore, in a realistic picture of transport that is damped by water, the charge configuration changes relatively slowly and the frequency of field updates can be relaxed without appreciably perturbing the pair correlation function.

Careful benchmarking is necessary to determine the optimal frequency for field updates and that benchmarking needs to be done for the range of ions and concentrations and conditions of interest. Figure 9(a) shows the anion–anion and cation–anion pair correlation functions for a 1 M monovalent solution, computed using progressively longer time intervals between solutions of Poisson's equation. As shown, the time between Poisson updates can be relaxed to a few picoseconds before any significant distortion in the pair correlation function is evident. Also shown in figure 9(b) are cation–cation and cation–anion

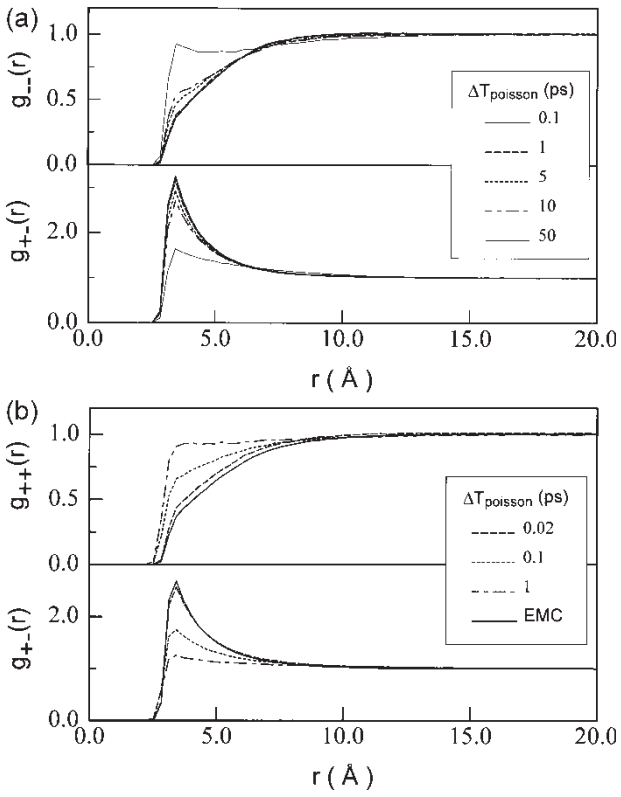

Figure 9. Relaxing the frequency of Poisson equation solution. Pair correlation functions computed for a 1 M monovalent electrolyte of ions consisting of two equally sized ion species. *Top*: $g_{-}(r)$ and $g_{+-}(r)$ computed for $\Delta T_{\mathrm{poisson}} = 0.1$, 1, 5, 10 and 50 ps. *Bottom*: Scattering rates reduced by factor of 100, $g_{++}(r)$ and $g_{+-}(r)$ computed for $\Delta T_{\mathrm{poisson}} = 20$, 0.1 and 1 ps.

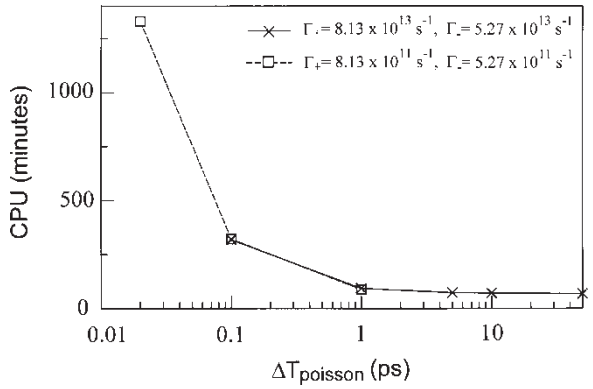

Figure 10. CPU time as a function of $\Delta T_{\mathrm{poisson}}$ for the pair correlation function calculations in figure 9.

pair correlation functions computed using ion–water scattering rates reduced by a factor of 100, with the EMC result included for comparison. Since the lower scattering rate allows the ions to diffuse much further over the same time scale, Poisson's equation needs to be resolved much more frequently. The corresponding run-times for each simulation are shown in figure 10. Again we observe the speed-up saturating beyond a certain point, in this case at Poisson update intervals of 1 ps, because particle transport and pair correlation calculations start to dominate the workload.

The results in figure 9 were computed using the P^3M scheme on a $\Delta = 2$ Å mesh. Similar benchmark calculations performed on a $\Delta = 4$ Å mesh indicate that the time between Poisson updates can be relaxed out even further before the pair correlation function becomes compromised. This stands to reason since the time scale over which the charge distribution on the mesh changes appreciably is longer on the coarser mesh. It should also be noted that although the results in figure 9 suggest that Poisson's equation can be solved relatively infrequently with respect to the ion trajectory integration time-step, this result has only been validated for equilibrium conditions. Ion channel systems are far from equilibrium, having regions of very high fixed charge with very little Coulombic screening. In such high-field regions ion transport is unlikely to be completely diffusive and transport coefficients are not necessarily the same as for bulk conditions. We therefore caution against relaxing the time interval between solving Poisson without first performing benchmark simulations.

4. Simulation of the Gramicidin ion channel

We now return to the original motivation behind the development of the BioMOCA code—to develop a feasible alternative to Molecular Dynamics for the simulation of ion transport through protein channels. In this section, we present a full-scale BioMOCA simulation of ion transport through the gramicidin A (gA) ion channel embedded in a lipid membrane. The gramicidin molecule

consists of 15 amino acids folded into a helical structure. When two gramicidin molecules align end-to-end to create a dimer, a narrow channel approximately 25 Å long and 4 Å in diameter is formed, allowing the conduction of small monovalent cations. Because of its small and relatively simple structure and the ease with which it can be synthesized, gramicidin has been well studied [58,61,62], both experimentally [55,56,59,60,84,88,89] and theoretically [11,59,72], and is a popular model channel on which to develop a prototype channel simulation [11,17,18,21,22,40,57,63,64,72]. There exist several published structures for gramicidin. For this particular work we used the 1 MAG.pdb structure determined via solid-state NMR by Ketchem *et al.* [83]. The partial charges residing on the protein atoms are taken from the GROMOS force field.¶ A 2D slice through the 3D BioMOCA representation of the channel system is shown in figure 2. The sensitivity to the chosen structure and force field is great and is the subject of much discussion [57].

As discussed earlier, due to the size and conformation of the gramicidin channel, the motion of water molecules inside the channel pore is very restricted and this has led to a lack of understanding regarding some of the physical constants that characterize the channel in the simulation, e.g. dielectric and diffusion coefficients. Further insight into these issues may be anticipated from MD simulations. However, for the present work the three distinct regions—lipid, protein and electrolyte (baths and channel pore)—were assigned dielectric coefficients of $\varepsilon = 2$, 20 and 80, respectively. Since run-times are dominated by the repeated solution of Poisson's equation, we have employed a dual mesh system in which the region accessible to ions is defined on a fine $\Delta = 0.5$ Å mesh while the fields are solved on a coarser $\Delta = 1$ Å mesh. This allows for manageable run-times while still retaining as much structural detail as possible. For the results presented here, we used a Poisson mesh of $25 \times 25 \times 74$ grid points and a steric mesh of $49 \times 49 \times 103$ grid points, creating a domain 73 Å in length and 24 Å in height and width. Since steric effects are only important in the region containing the protein and lipid, the steric mesh can be a sub-domain of the whole simulation domain.

Several simulations of Na^+ and Cl^- transport were performed using scattering rates determined from published ion diffusion coefficients measured in bulk electrolyte [81]. The scattering rates are high, $\lambda_+ = 8.13 \times 10^{13}\,s^{-1}$ and $\lambda_- = 3.46 \times 10^{13}\,s^{-1}$, necessitating small time-steps of 10 fs. It should be noted that while these scattering rates are correct for bulk electrolyte, the appropriate values to use inside the channel environment is still an open question. MD simulations can provide detailed trajectory information from which space-dependent diffusion coefficients can be extracted; however, the values thus obtained contain contributions from both ion–water and ion–protein scattering events. In BioMOCA the two interactions are handled separately, with ion–water interactions modeled as thermalizing scattering events and ion–protein steric interactions modeled as hard-wall diffusive reflections, and it is not clear how to extract the ion–water scattering component from the total diffusion coefficient obtained from MD simulations. Therefore, for the present work we have used bulk diffusion coefficients inside the pore region. The high scattering rates have some advantageous effects also. As discussed in the previous section, since the ions diffuse very slowly, the charge distribution on the coarser mesh does not change appreciably during one time-step, allowing the frequency with which Poisson's equation is solved to be relaxed. For this work we solve Poisson's equation every 100 time-steps (1 ps), in addition to whenever an ion enters or leaves the system. The latter condition leads to Poisson's equation being solved much more frequently than 1 ps. With these numerical parameters and mesh configurations the CPU requirements are fairly modest: approximately 24 CPU hours on a Pentium III (1 GHz) for 50–60 ns of simulation time. RAM requirements are less than 100 MB.

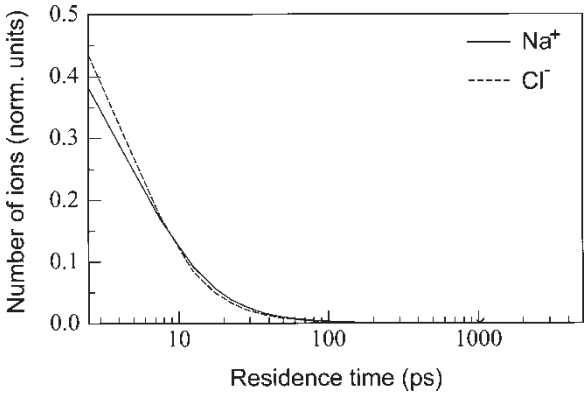

Figure 11. Distribution of ion residence times (trajectory duration) accumulated from 16 separate simulations of average duration 162 ns (total simulation time ≈ 2.6 μs).

One of the main computational problems facing particle-based simulations of ion conduction in protein channel systems is the fact that for most ion channels, ion trajectories that successfully cross the membrane through the channel pore are extremely rare events. Thus, computing channel conductance directly by counting ion crossings involves tracking a huge number of trajectories, most of which never go anywhere near the mouth of the channel. This issue is most clearly illustrated in figures 11 and 12, which show respectively, the distribution of ion residence times (i.e. duration of trajectory) and the distribution of trajectory lifetimes for those ions that successfully crossed the channel, obtained from 16 separate simulations of average duration 162 ns. Each simulation was performed with the same parameters: 250 mV bias applied at the right-hand-side contact, 1 M

¶http://www.igc.ethz.ch/gromos/

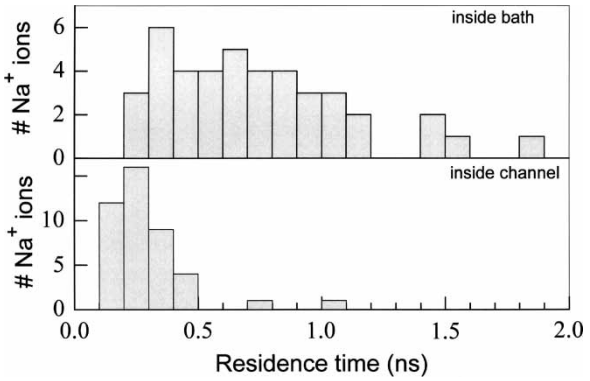

Figure 12. Distribution of residence times for ions that successfully crossed the channel, accumulated from 16 separate simulations lasting between 147 and 182 ns. The top half of the figure shows the amount of time spent in the bath regions between the contact and membrane while the lower half shows the amount of time spent inside the channel.

NaCl in each electrolyte bath. The cumulative duration of all the simulations was approximately 2.6 μs. Figure 12 also shows the breakdown of how much time was spent in each bath (top) as well as inside the channel itself (bottom). As figure 11 shows, less than 12% of the Na^+ ions remain in the bath longer than 100 ps and fewer than 3% remain longer than 1 ns. On the other hand, from figure 12, we see that those ions that do make it across the channel typically remain in the system for a few nanoseconds, most of which is spent diffusing in the baths. The system is so highly collisional that ions typically require on the order of several hundred picoseconds to diffuse from the contact region to within ≈5 Å of the edge of the membrane, and another several hundred picoseconds to actually enter the mouth of the channel. Furthermore, of those ions that do reach the vicinity of the membrane, only a very few actually go anywhere near the pore, as indicated by figure 13, which shows the distribution of the maximum distance from the contact that the ion reached during its trajectory. Fewer than 4% of the ions ever get within a few Angstroms of the lipid membrane, and the sharp peaks approximately 23–25 Å from the contacts indicate that most those ions do not actually enter the channel.

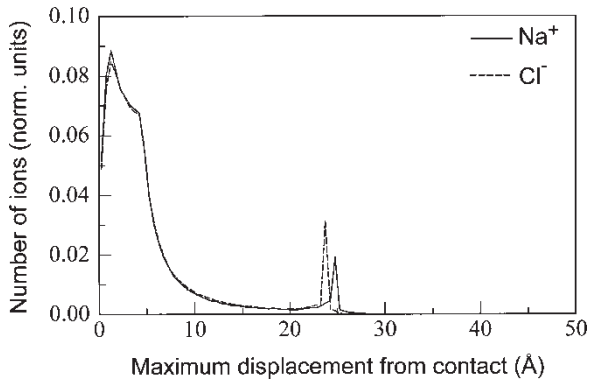

Figure 13. Distribution of the furthest distance from the contact reached by all ions during ≈2.6 μs of total simulation time.

The question then remains how one can reliably estimate the channel current in the simulation. For small systems like the gramicidin channel, which draws currents of the order of a only few pA, the brute force approach of counting the number of ions crossing the channel requires simulation times of the order of several microseconds in order to yield reliable statistics. With the resources currently available a single simulation lasting 5 μs could take a few months. However, if we restrict ourselves to simulations of steady-state current, where any transient behavior is strictly numerical in nature, we can employ the principle of time parallelization to distribute the total simulation time $T_{\text{tot}}^{\text{sim}}$ across several processors, with each processor simulating a smaller window of time T_i^{sim}, subject to the following two conditions: T_i^{sim} must be much greater than the initial transient in each simulation, and long enough to observe a statistically acceptable number of ions crossing the channel. For the gramicidin simulation conditions cited above the latter requirement necessitates $T_i^{\text{sim}} \approx$ several hundred nanoseconds, while the system initial transient is typically much less than 1 ns. Combining the statistics from each independent simulation significantly reduces the variance in the estimated channel current, with a speed-up and variance reduction determined by $(T_{\text{tot}}^{\text{sim}}/T_i^{\text{sim}})$. To demonstrate this approach we performed a gramicidin simulation of total duration 4.3 μs distributed across 16 Intel processors (1 GHz) with T_i^{sim} ranging from 235–300 ns, using the same physical parameters as cited above, *viz.*, 250 mV bias applied at the right-hand-side contact and 1 M NaCl in each electrolyte bath. The total wall clock time required was approximately 120 h. Figure 14 shows the histogram of Na^+ currents estimated from each simulation. Combining the statistics from each simulation gives an estimated current of 3.85 ± 0.97 pA which is comparable with the current measured experimentally under similar conditions. Single-channel current-voltage measurements of gramicidin in 1 M NaCl yield currents at approximately 2.5 pA under an applied bias of 200 mV [84]. The mean value of 3.85 ± 0.97 pA corresponds to 7.2 ± 1.8 Na^+ crossings per 300 ns.

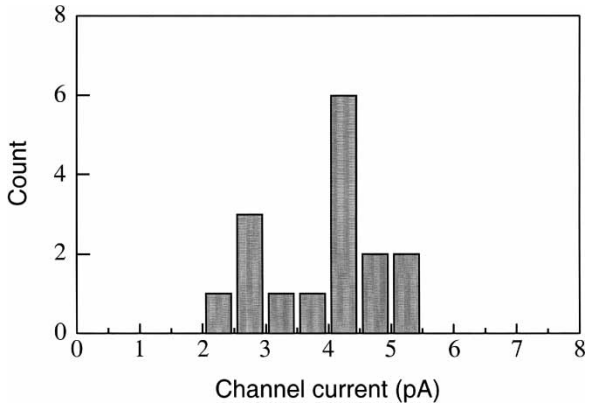

Figure 14. Histogram of Na^+ currents estimated from 16 separate simulations of duration ranging from 235 to 300 ns, totaling 4.3 μs. The mean value of 3.85 ± 0.97 pA corresponds to 7.2 ± 1.8 Na^+ crossings per 300 ns of simulation time.

During the total 4.3 μs of simulation time 104 Na^+ ions were observed to cross the channel, all in the direction consistent with the applied bias, i.e. from the right-hand-side bath to the left-hand-side bath, whereas no Cl^- ion crossings were observed whatsoever. This result can be easily explained by considering the size of the Cl^- ion (ionic radius = 1.8 Å) which is almost as large as the pore cross-section itself (radius ≈ 2 Å), making it nearly impossible for the Cl^- ion to enter the channel. To check this assertion, we artificially set the Cl^- ionic radius to the same value as the Na^+ ion (0.95 Å) and ran several additional simulations under otherwise identical conditions. During a total of 2 μs of simulation 50 Na^+ ions crossed the channel, while 9 reduced radius Cl^- ions crossed the channel in the opposite direction, thus constituting approximately 15% of the total channel current. However, when we reverse the situation and set both Na^+ and Cl^- radii to 1.8 Å no ions of either species were observed to cross the channel. This therefore indicates that although ionic size is the main reason that gramicidin blocks Cl^- ions, electrostatic factors also contribute to the selectivity. This will be discussed further in the following section.

In Figures. 15–17, we show the Na^+ concentration (figure 15), Cl^- concentration (figure 16) and potential (figure 17), averaged over the entire 4.3 μs of simulation time, on a 2D slice cutting through the center of the channel. The channel geometry can be seen more distinctly in panel (a), while the 3D image in panel (b) gives a clearer picture of the spatial variations in concentration and potential. The corresponding 1D line plots, constructed from the 3D ion concentration data by averaging over the plane perpendicular to the channel, and extracted from the 3D potential data along the center of

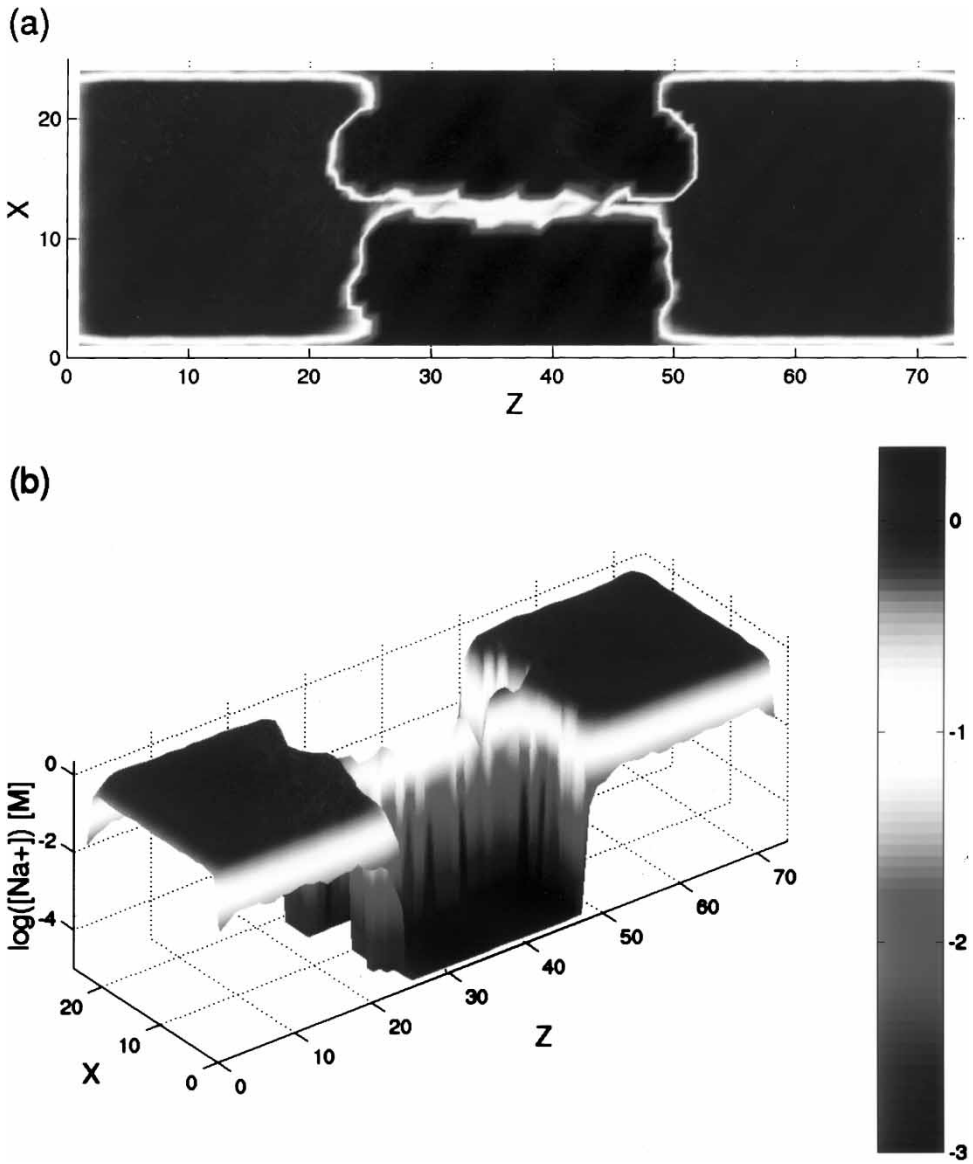

Figure 15. Na^+ concentration averaged over 4.3 μs of simulation time, on a 2D slice cutting through the center of the channel. All dimensions are in Ångstroms and concentration is plotted in Moles/Litre (M) on a logarithmic scale, with the indices indicated alongside the colour bar. All values below 10^{-3} are shown at the same level.

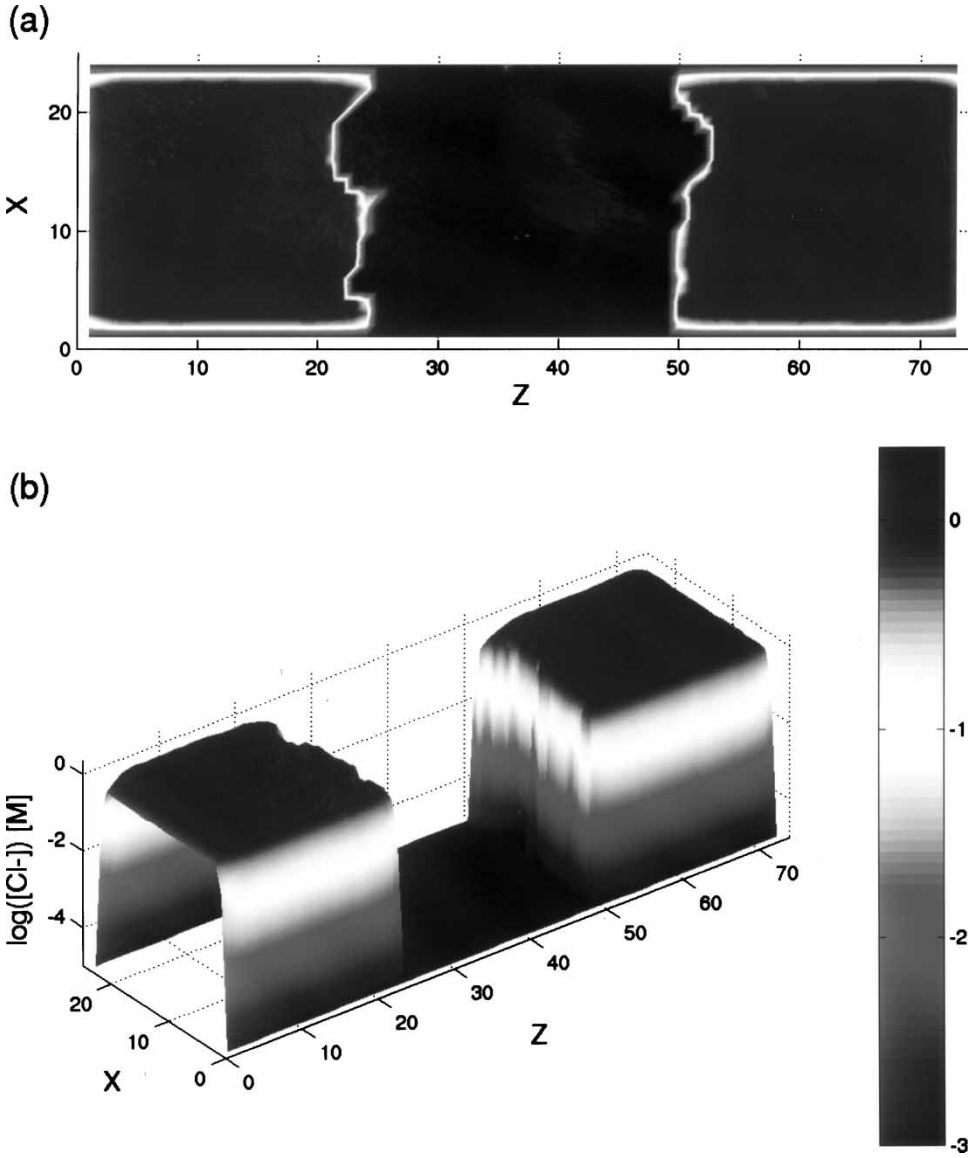

Figure 16. Cl^- concentration averaged over 4.3 μs of simulation time, on a 2D slice cutting through the center of the channel. All dimensions and scales are identical to those in figure 15.

the channel, are shown in figure 18. The main points to note are as follows: The average concentration of both species in the baths remains flat at ≈ 1 M demonstrating that the contact region model is properly implemented. Inside the narrow pore region the Na^+ concentration drops by more than an order of magnitude while Cl^- is excluded altogether. Because the channel presents a severe bottleneck for Na^+ ion conduction, almost all the applied potential drops across the channel/membrane with only a negligible drop across the baths so that the channel acts essentially as a resistor.

5. Selectivity of the Gramicidin channel: some considerations

As discussed earlier in this paper, the issue of what values to assign to the dielectric coefficients of the channel protein and interior of the pore, and indeed the actual definition of the dielectric coefficient in the context of ion channel simulations, is presently unresolved. In the previous section, we presented results of a full-scale BioMOCA simulation of the gramicidin channel, using $\varepsilon_p = 20$ for the dielectric coefficients in the protein and $\varepsilon_{ch} = 80$ in the channel pore, values which are arguably too high [69], and a distribution of fixed charge on the protein taken from the GROMOS force field. With these assumptions the absolute exclusion of Cl^- ions from the pore could be explained from simple steric considerations. Further simulations also demonstrated that Cl^- ions will enter the channel if their radii are reduced to the same size as Na^+; however the Cl^- current is still much lower than the Na^+ current, indicating additional factors also play a role in gramicidin's selectivity. Adding weight to this argument is the experimental observation that gA only conducts small monovalent cations, an aspect that cannot be explained by

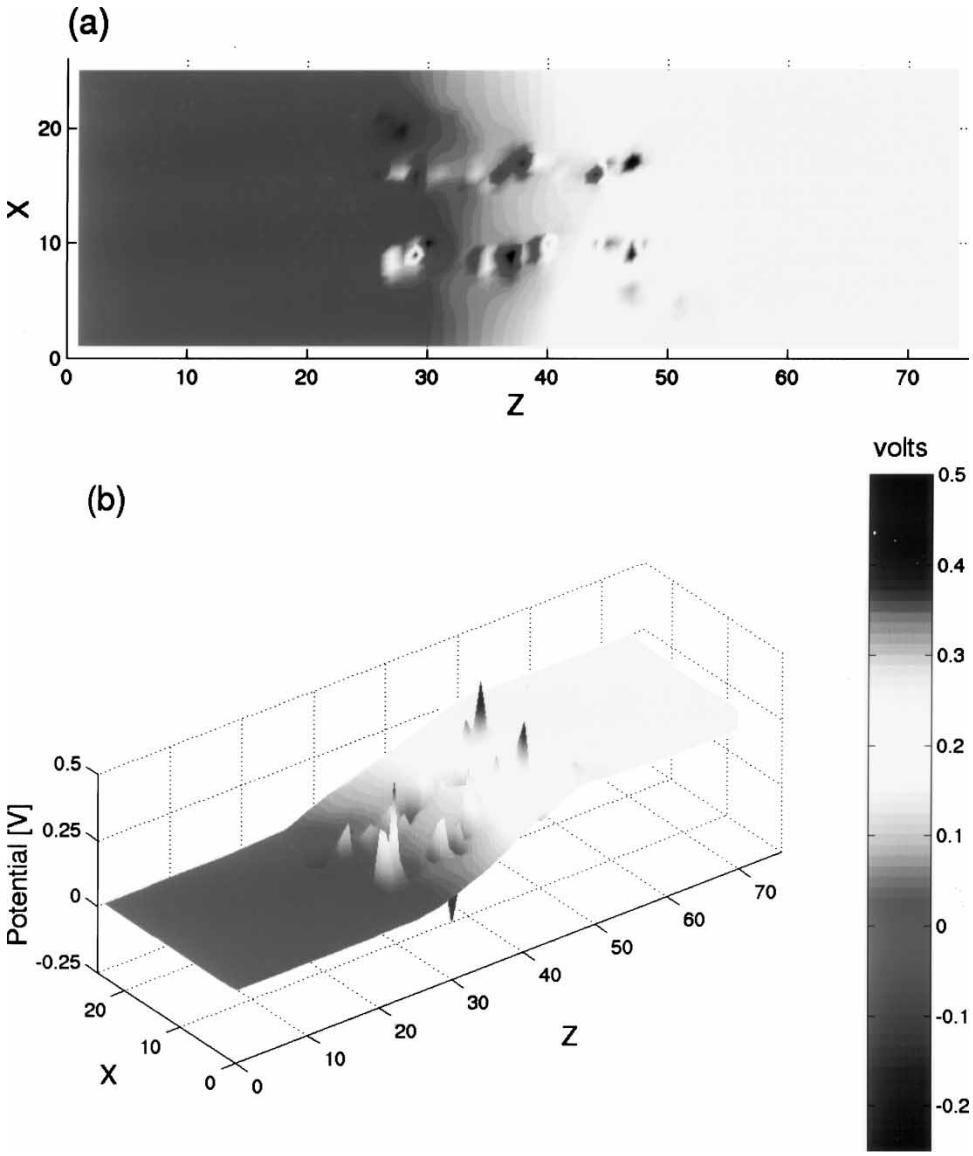

Figure 17. Electrostatic potential averaged over 4.3 μs of simulation time, on a 2D slice cutting through the center of the channel. All dimensions are in Ångstroms.

ion size. Gramicidin does not conduct Ca^{2+} ions, for example, despite the fact that at 0.99 Å the ionic radius of Ca^{2+} is only marginally greater than that of Na^{+}.

Recently it has been proposed by Nadler *et al.* [63] and Edwards *et al.* [64] that the mechanism allowing gA to selectively conduct small monovalent cations while at the same time blocking anions and divalent cations lies in the permanent charge being distributed over the protein in such a way that it creates a potential energy well that counteracts the DBF—the force exerted on a charge as it approaches a boundary between two regions of differing dielectric coefficient, due to the image charge induced on the other side of the boundary. The sign and magnitude of the DBF depend on the relative values of the dielectric coefficients in the two regions as well as on geometric factors, and the magnitude scales as the square of the magnitude of the point charge. For the gramicidin channel/membrane system considered here, any point charge attempting to move from the bath to the channel pore along the central axis of the channel will experience a repulsive DBF, even though it never actually crosses any dielectric boundary. The 3D nature of the dielectric boundary between protein and aqueous regions causes the DBF arising from the induced charge in the protein to always have a component along the axis of the channel, creating a potential energy barrier for all ion species attempting to traverse the channel regardless of the sign of the charge. Due to the double charge on divalent ions this barrier is much higher than for monovalent ions.

Both Nadler *et al.* [63] and Edwards *et al.* [64] argue that for monovalent cations the energy barrier arising from the DBF is almost cancelled by a potential energy well created by the permanent charge on the protein, while for anions and divalent cations the sum of the two contributions results in an insurmountable energy barrier that prevents conduction. Although this hypothesis was

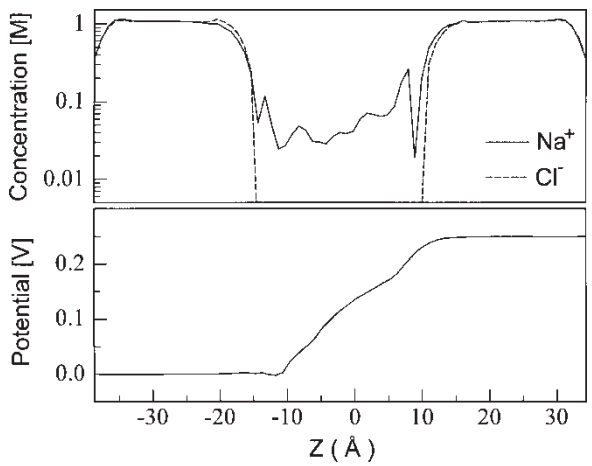

Figure 18. 1D profiles of time-averaged Na^+ and Cl^- concentration and potential, constructed from the 3D ion concentration data by averaging over the plane perpendicular to the channel, and extracted from the 3D potential data along the center of the channel.

arrived at by considering the potential energy profiles for single point charges moving along the axis of the channel, thereby ignoring the possibility of Coulombic shielding from other ions near the channel, it is reasonable to expect electrostatics to also play a role in gramicidin's selectivity. In this section, we continue this line of inquiry, and demonstrate that the potential energy profile for a single ion attempting to cross the channel is exquisitely sensitive to the particular choice of dielectric coefficients and partial charges, the values of which are not known with any degree of certainty.

Figure 19 shows the net potential energy profiles for a single point charge Na^+ (solid line) and a single point charge Cl^- (dashed line) ion, as they each pass separately through the center of the same gramicidin channel system described in the previous section (see figure 2), derived from the 1 MAG.pdb structure and the GROMOS force field. The lipid, protein and

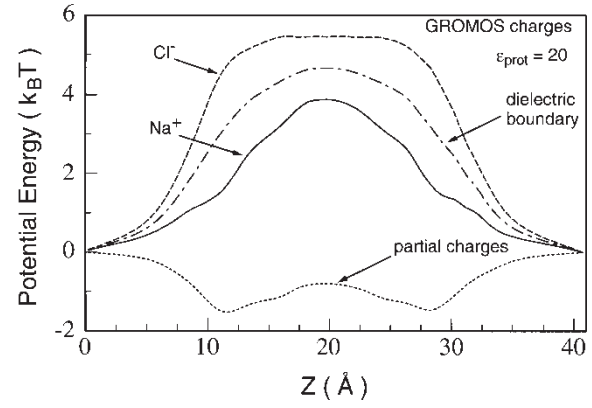

Figure 19. Net potential energy profiles for a single point charge Na^+ (solid line) and a single point charge Cl^- (dashed line) ion, passing separately through the center of the gA channel system. Partial charges take from the GROMOS force field. The lipid, protein and electrolyte dielectric coefficients were assigned values of $\varepsilon = 2$, 20 and 80. Individual contributions from the partial charges (dotted line) and DBF (dash-dot line) are also shown.

electrolyte dielectric coefficients were assigned values of $\varepsilon = 2$, 20 and 80, respectively and Poisson's equation was solved on a $\Delta = 1$ Å mesh. Individual contributions from the partial charges and DBF are also indicated respectively by the dotted and dash-dot lines. Both ions experience the same barrier of $\approx 4.7\,k_BT$ due to the DBF. However, for Na^+ this barrier is partially cancelled by the double potential well roughly $1.5\,k_BT$ deep created by the permanent charges on the protein, resulting in a net potential energy barrier $\approx 3.8\,k_BT$, while for Cl^- the permanent charges present an additional barrier which adds to the dielectric barrier resulting in a net potential energy barrier roughly $5.5\,k_BT$ high. Nonetheless, as demonstrated by the BioMOCA simulations in the previous section, these relatively moderate potential energy barriers can be overcome to permit ion conduction if a sufficiently high bias (e.g. 250 mV $\approx 9.7\,k_BT$) is applied across the system. Indeed, if ion size effects are disregarded (e.g. by setting the Cl^- radius equal to the Na^+ radius) then the partial selectivity observed in the BioMOCA simulations (only 15% of the total current is carried by Cl^- ions) may be attributed to the fact that the Cl^- ion faces a higher barrier than Na^+ ions.

Although the potential energy profiles in figure 19 are consistent with the channel favoring cation over anion conduction, they do not support the explanation of gramicidin's complete exclusion of anions suggested by Nadler *et al.* [63] and Edwards *et al.* [64]. The net potential energy profiles presented in [63] show a similar barrier to Na^+ conduction ($\approx 5\,k_BT$) but a much higher ($\approx 12.5\,k_BT$) barrier for Cl^- conduction, while those presented in Ref. [64] indicate a shallow potential double well roughly $1.5\,k_BT$ deep for Na^+ and a huge barrier for Cl^- about $24\,k_BT$ high. However both groups assumed a value of $\varepsilon_p = 2$ for the dielectric coefficient of protein rather than the higher value of $\varepsilon_p = 20$ used here. As discussed earlier the appropriate value to use for the protein dielectric depends critically on the specific channel model employed. The more physics that is explicitly included in the model then the lower the dielectric coefficient required. For coarse-grained particle models, such as BioMOCA, the use of $\varepsilon_p = 2$ is arguably too low but $\varepsilon_p = 20$ is also probably unrealistically high. For the sake of comparison however we now consider a lower value of $\varepsilon_p = 2$. In this case, as shown in figure 20, the dielectric barrier created by the protein increases to $\approx 12\,k_BT$ while the potential well due to the permanent charges on the protein is only $\approx 4\,k_BT$. The resulting net potential energy profiles are now much greater for both Na^+ ($\approx 9\,k_BT$) and Cl^- ($\approx 15\,k_BT$).. In this situation, we can expect the channel conductivity to be much lower and indeed during a total simulation time of 2 μs only 5 Na^+ ions were observed to cross the channel under a 250 mV bias which amounts to negligible current (<0.4 pA). In order to facilitate conduction of either species a substantially higher applied bias ($\approx$500 mV) would be required to overcome such high energy barriers. Almost

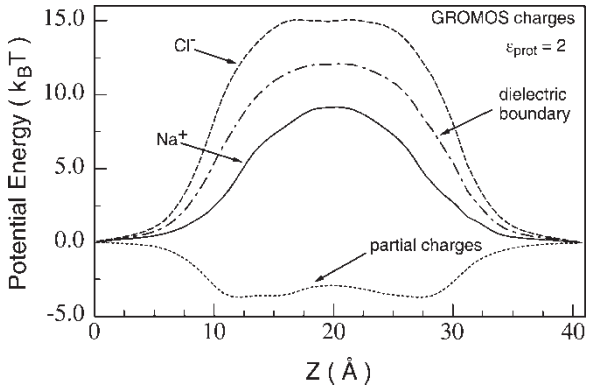

Figure 20. Net potential energy profiles for a single point charge Na^+ (solid line) and a single point charge Cl^- (dashed line) ion, passing separately through the center of the gA channel system. Partial charges take from the GROMOS force field. The lipid, protein and electrolyte dielectric coefficients were assigned values of $\varepsilon = 2$, 2 and 80. Individual contributions from the partial charges and DBF are shown by the dotted and dash-dot lines, respectively.

all lipid bilayers will break down under such high voltages. Gramicidin conductance and selectivity cannot be explained using this combination of force fields and dielectric coefficients. We therefore now turn our attention to the permanent charge distributions used in each study. There exists in the literature several different force fields that parameterize the distribution of permanent charge on each amino acid. The partial charges used by Nadler *et al.* [63] were taken from the OPLS force field [85,86], while Edwards *et al.* [64] employed the PARAM22 version of the CHARMM force field [87]. On the other hand all the results presented here thus far were computed using partial charges from the GROMOS force field.¶ To illustrate the sensitivity of the energy landscape inside the channel to the charge distribution on the protein we replaced the GROMOS charges with those from the CHARMM force field and recomputed the potential profiles, again using $\varepsilon_p = 2$ in the protein. As shown in figure 21, the height of the DBF barrier does not alter appreciably, since the dielectric boundary is almost the same in both cases. The slight difference ($\approx 1\,k_BT$) between the two dielectric barrier profiles is the result of a small difference between the Poisson meshes used in each case. However, the potential well due to the CHARMM charges is now $\approx 10\,k_BT$ deep compared to the $\approx 4\,k_BT$ produced by the GROMOS charges, which lowers the total barrier for Na^+ to $\approx 1\,k_BT$ at the same time increasing the Cl^- barrier to $\approx 20\,k_BT$. These potential energy profiles are now consistent with the picture of selectivity suggested by both Edwards *et al.* [64] and Nadler *et al.* [63].

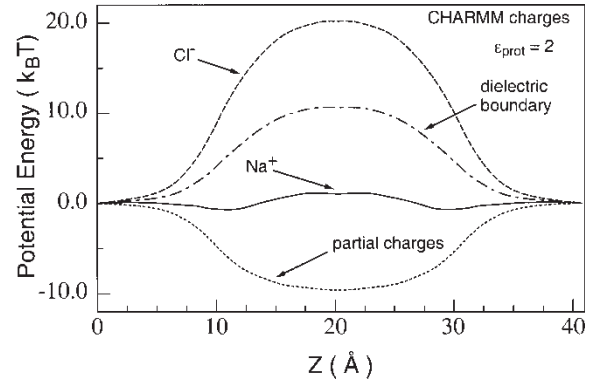

Figure 21. Net potential energy profiles for a single point charge Na^+ (solid line) and a single point charge Cl^- (dashed line) ion, passing separately through the center of the gA channel system. Partial charges take from the CHARMM force field. The lipid, protein and electrolyte dielectric coefficients were assigned values of $\varepsilon = 2$, 2 and 80. Individual contributions from the partial charges (dotted line) and DBF (dash-dot line) are also shown.

Comparing the potential energy profiles computed using GROMOS partial charges (figure 20) and CHARMM partial charges (figure 21) demonstrates clearly that although gA is charge neutral overall, differences in the way the permanent charge is actually distributed over the protein can lead to dramatically different potential energy profiles for both Na^+ and Cl^- ions, and consequently different conclusions regarding channel selectivity and conductance. The main differences between the GROMOS and CHARMM partial charges reside in the charge distribution on the peptide backbone, which line the channel pore, and the side-chains of the Tryptophan (TRP) amino acid groups. Each gramicidin monomer has four TRP groups located near the entrance of the channel which are known to play an important role in the channel's conductance properties. Mutation experiments that involve replacing TRP residues with various other groups having different permanent dipole moments have shown gA conductivity to be very sensitive to strength and orientation of the side-chain dipole moments at those specific locations in the protein [84,88,89]. Specifically, substitutions that lowered the overall dipole moment in those locations were found to lower the channel conductivity several-fold. These findings are consistent with the simulation results reported here. In the CHARMM partial charge set the dipole moments of the carbonyl and NH bonds in the peptide bonds, and the TRP side-chains are significantly stronger than those of the GROMOS force field. Full 3D simulations lasting 2 μs performed with the CHARMM charges yielded Na^+ currents that were more than an order of magnitude greater than those computed using the GROMOS charges. Nonetheless, with the assumption of $\varepsilon = 2$ for the dielectric coefficient in the protein and lipid, and $\varepsilon = 80$ for the dielectric coefficient in the electrolyte bath and inside the channel pore, neither set of partial charges could yield currents that were comparable to experiment. As discussed earlier, a value of $\varepsilon_p = 2$ for the dielectric coefficient in the protein is arguably too low, while assuming the value for bulk water ($\varepsilon_w = 80$) inside the pore is clearly unrealistically high. It has been proposed that by using $\varepsilon_p = 5$ for the dielectric coefficient in the protein it may be possible to encompass the contribution of conformational changes to the protein's dielectric response [67]. Following this suggestion we computed potential energy profiles with $\varepsilon_p = 5$ in

the protein and $\varepsilon_{ch} = 20$ inside the pore, and found the DBF barrier increased to roughly $40\,k_B T$. Although the calculation assumed an unphysical step function transition in the dielectric coefficient going from bath to pore, it does drive home the point that a thorough handle on the structural, electrostatic and dielectric properties of the gA protein channel system are required before any quantitatively meaningful statements about ion conduction and selectivity can be made. Furthermore, we have investigated only two of many factors that influence channel behaviour *viz.*, dielectric coefficients and partial charges. There are numerous other physical factors that will undoubtedly affect the channel behaviour e.g. diffusion coefficients, dehydration energies, some of which are beyond the scope of the present generation of coarse-grained particle models.

6. Discussion

We have introduced BioMOCA, a 3D ion channel simulator based on the Boltzmann Transport Monte Carlo/particle–particle–particle-mesh (BTMC/P^{3}M) methodologies as an alternative to the computationally intensive Molecular Dynamics approach for simulating ion transport through protein channels. The model retains the essential particle nature of the ions but treats water, protein and membrane as a continuum, thus enabling simulation times to extend to several microseconds, well beyond the present limit of MD simulations. In addition, unlike almost all MD simulations, the BioMOCA simulator does not employ periodic boundary conditions, making it eminently suitable for simulating ion transport in generalized device structures.

Before embarking on full-scale ion channel simulations we first demonstrated the validity of the BTMC/P^{3}M methodology for electrolytes by using BioMOCA to compute the ion–ion pair correlation function for several model electrolytes under bulk equilibrium conditions and comparing the results to benchmark calculations performed using the well-established EMC methodology. The latter approach is computationally very efficient but, through its assumption of equilibrium conditions, is limited to providing information on the system configuration. The excellent agreement between the two approaches lends confidence in our implementation of the short-range ion–ion interactions algorithm in BioMOCA. We have also shown that the computational performance of BioMOCA can be dramatically improved if the P^{3}M scheme is implemented carefully. This has extremely important implications for realistic simulations of computationally large systems such as those encountered in ion channel systems with physically realistic electrolyte baths. A good compromise must be achieved in the choice of mesh size so that the overhead of evaluating the Coulomb forces explicitly on a short-range domain for each particle does not outweigh the speed-up achieved from using a coarser mesh for the particle-mesh scheme. The P^{3}M scheme is currently implemented in such a way that while the distance over which the modified Lennard-Jones ion–ion interaction is included is greater than the range over which the particle–particle Coulomb interaction is calculated explicitly, the overhead associated with searching for ions in the latter domain is negligible. For regions near equilibrium we have also shown that if the ion–water scattering rate is sufficiently high the charge configuration changes sufficiently slowly to relax the time interval between successive solutions of Poisson's equation to several picoseconds without any noticeable change to the pair correlation function.

Preliminary simulations of Na^+ transport through the gramicidin A channel yielded currents that compare reasonably well with experimental measurements given the level of approximations inherent in the model. In addition, the absolute exclusion of Cl^- from the channel pore could be explained from steric considerations alone. These results were however obtained using specific values for the ion diffusion coefficients inside the channel pore, partial charges residing on the protein and dielectric coefficients in the protein, lipid and channel pore, none of which are known with any degree of certainty. Not surprisingly, the potential energy profiles computed for single point charges passing through the center of the channel were found to vary dramatically depending on the value assigned to the dielectric coefficients in the protein. Decreasing the latter from $\varepsilon_p = 20$ to $\varepsilon_p = 2$ leads to a substantial increase in the potential energy barrier for Na^+, and a correspondingly large drop in the computed current. Likewise, potential energy profiles and channel currents were found to be extremely sensitive to the choice of force field. For example, using partial charges taken from the CHARMM/PARAM22 force field yielded Na^+ currents that were more than order of magnitude greater than those obtained using partial charges from the GROMOS force field. Until reliable values are available for the aforementioned physical quantities, we advocate treating them as tunable parameters, bearing in mind that any conclusions regarding channel behavior derived from simulations must be interpreted strictly within the framework of assumptions upon which the simulation is based.

Finally, while an implicit water model appears to be sufficient in the bath regions, it may not be appropriate in the narrow gA pore where single-filing effects almost undoubtedly influence ion dynamics and the dielectric coefficient is difficult to define. Molecular Dynamics simulations may provide crucial insight in this region, and indeed a hybrid BTMC/P^{3}M-MD approach, in which implicit water electrolyte baths are bridged to a Molecular Dynamics model of the channel pore, may well be required if one is seriously pursuing a quantitatively realistic simulation of channel behavior. Nonetheless, in its present incarnation the BioMOCA simulator is a promising predictive tool for studying conduction through ionic channels on a timescale relevant to experimental observations.

Acknowledgements

This work was supported by financial grants from the National Science Foundation — Network for Computational Nanotechnology (Grant No. EEC-0228390), Defense Advanced Research Projects Agency (DARPA SIMBIOSYS AF NA 0533) and by the National Center for Supercomputing Applications (NCSA).

References

[1] B. Alberts, D. Bray, J. Lewis, M. Raff, K. Roberts, J.D. Watson. *Molecular Biology of the Cell*, Garland, New York (1994), p. 1294.
[2] F.M. Ashcroft. *Ion Channels and Disease*, Academic Press, New York (1999), p. 481.
[3] B. Hille. *Ionic Channels of Excitable Membranes*, Sinauer Associates Inc., Sunderland (2001), Ch. 1.
[4] E.C. Conley. *The Ion Channel Facts Book. I. Extracellular Ligand-gated Channels*, Academic Press, New York (1996), p. 425.
[5] E.C. Conley. *The Ion Channel Facts Book. II. Intracellular Ligand-gated Channels*, Academic Press, New York (1996), p. 776.
[6] B. Eisenberg. Ion channels as devices. *J. Comput. Electron.*, **2**, 245 (2003).
[7] J. Sambrook, D.W. Russell. *Molecular Cloning: A Laboratory Manual (3-Volume Set)*, 3rd Ed., Cold Spring Harbor, New York (2001).
[8] J.D. Watson, T.A. Baker, S.P. Bell, A. Gann, M. Levine, R. Losick. *Molecular Biology of the Gene*, 5th Ed., Benjamin/Cummings, (2003).
[9] T. Schlick. *Molecular Modeling and Simulation*, Springer Verlag, New York (2002), p. 656.
[10] D.P. Tieleman, P.C. Biggin, G.R. Smith, M.S. Sansom. Simulation approaches to ion channel structure-function relationships. *Q. Rev. Biophys.*, **34**, 473 (2001).
[11] B. Roux, M. Karplus. Ion transport in a gramicidin-like channel: Dynamics and mobility. *J. Phys. Chem.*, **95**, 4856 (1991).
[12] W. Im, B. Roux. Ions and counterions in a biological channel: a molecular dynamics simulation of OmpF porin from *Escherichia coli* in an explicit membrane with 1 M KCl aqueous salt solution. *J. Mol. Biol.*, **319**, 1177 (2002).
[13] B. Roux, T. Allen, S. Bernéche, W. Im. Theoretical and computational models of biological ion channels. *Q. Rev. Biophys.*, **37**, 15 (2004).
[14] S. Selberherr. *Analysis and Simulation of Semiconductor Devices*, Springer-Verlag, Vienna (1984).
[15] V. Barcilon. Ion flow through narrow membrane channels: Part I. *SIAM J. Appl. Math.*, **52**, 1391 (1992).
[16] V. Barcilon, D.P. Chen, R.S. Eisenberg. Ion flow through narrow membranes channels: Part II. *SIAM J. Appl. Math.*, **52**, 1405 (1992).
[17] M.G. Kurnikova, R.D. Coalson, P. Graf, A. Nitzan. A lattice relaxation algorithm for 3-D Poisson–Nernst–Planck Theory with application to ion transport through the Gramicidin A channel. *Biophys. J.*, **76**, 642 (1999).
[18] A.E. Cardenas, R.D. Coalson, M.G. Kurnikova. Three-dimensional Poisson–Nernst–Planck Studies. Influence of membrane electrostatics on Gramicidin A Channel Conductance. *Biophys. J.*, 79 (2000).
[19] D.P. Chen, J. Lear, R.S. Eisenberg. Permeation through an open channel. Poisson–Nernst–Planck theory of a synthetic ionic channel. *Biophys. J.*, **72**, 97 (1997).
[20] R.S. Eisenberg. Computing the field in proteins and channels. *J. Membrane Biol.*, **150**, 1 (1996).
[21] U. Hollerbach, D.P. Chen, D.D. Busath, R.S. Eisenberg. Predicting function from structure using the Poisson–Nernst–Planck equations: sodium current in the Gramicidin A channel. *Langmuir*, **16**, 5510 (2000).
[22] U. Hollerbach, D.P. Chen, R.S. Eisenberg. Two- and three-dimensional Poisson–Nernst–Planck simulations of current flow through Gramicidin-A. *J. Sci. Comput.*, **16**, 373 (2001).
[23] Z. Schuss, B. Nadler, R.S. Eisenberg. Derivation of PNP equations in bath and channel from a molecular model. *Phys. Rev. E*, **64** (2001) 036116 1.
[24] T.A. van der Straaten, J.M. Tang, R.S. Eisenberg, U. Ravaioli, N. Aluru. Three-dimensional continuum simulations of ion transport through biological ion channels: Effect of charge distribution in the constriction region of porin. *J. Comput. Electron.*, **1**, 335 (2002).
[25] T.A. van der Straaten, J.M. Tang, U. Ravaioli, R.S. Eisenberg, N. Aluru. Simulating ion permeation through the OmpF Porin ion channel using three-dimensional drift-diffusion theory. *J. Comput. Electron.*, **2**, 29 (2003).
[26] W. Im, B. Roux. Ion permeation and selectivity of OmpF Porin: a theoretical study based on Molecular Dynamics, Brownian Dynamics, and Continuum Electrodiffusion theory. *J. Mol. Biol.*, **322**, 851 (2002).
[27] R.S. Eisenberg. From structure to function in open ionic channels. *J. Membr. Biol.*, **171**, 1 (1999).
[28] B. Corry, S. Kuyucak, S.-H. Chung. Tests of continuum theories as models of ion channels. II Poisson–Nernst–Planck Theory versus Brownian Dynamics. *Biophys. J.*, **78**, 2364 (2000).
[29] D. Boda, D.D. Busath, D. Henderson, S. Sokolowski. Monte Carlo simulations of the mechanism for channel selectivity: The competition between volume exclusion and charge neutrality. *J. Phys. Chem. B*, **104**, 8903 (2000).
[30] D. Boda, D. Henderson, D.D. Busath. Monte Carlo study of the effect of ion and channel size on the selectivity of a model calcium channel. *J. Phys. Chem. B*, **105**, 11574 (2001).
[31] D. Boda, D. Henderson, D.D. Busath. Monte Carlo simulation of the selectivity of calcium channels: improved geometrical model. *Mol. Phys.*, **100**, 2361 (2002).
[32] D. Boda, T. Varga, D. Henderson, D.D. Busath, W. Nonner, D. Gillespie, B. Eisenberg. Monte Carlo simulation study of a system with a dielectric boundary: application to a calcium channel selectivity. *Mol. Simul.*, **30**, 89 (2004).
[33] D. Boda, D.D. Busath, B. Eisenberg, D. Henderson, W. Nonner. Monte Carlo simulations of ion selectivity in a biological Na channel: charge-space competition. *Phys. Chem. Chem. Phys.*, **4**, 5154 (2002).
[34] S.C. Li, M. Hoyles, S. Kuyucak, S.H. Chung. Brownian dynamics study of ion transport in the vestibule of membrane channels. *Biophys. J.*, **74**, 37 (1998).
[35] S.H. Chung, M. Hoyles, T.W. Allen, S. Kuyucak. Study of ionic currents across a model membrane channel using Brownian dynamics. *Biophys. J.*, **75**, 793 (1998).
[36] S.H. Chung, T.W. Allen, M. Hoyles, S. Kuyucak. Permeation of ions across the potassium channel: Brownian dynamics studies. *Biophys. J.*, **77**, 2517 (1999).
[37] S.H. Chung, T.W. Allen, S. Kuyucak. Conducting-state properties of the KcsA potassium channel from molecular and Brownian dynamics studies. *Biophys. J.*, **82**, 628 (2002).
[38] K. Cooper, E. Jakobsson, P. Wolynes. The theory of ion transport membrane channels. *Prog. Biophys. Mol. Biol.*, **46**, 51 (1985).
[39] T. Schirmer, P.S. Phale. Brownian dynamics simulation of ion flow through porin channels. *J. Mol. Biol.*, **294**, 1159 (1999).
[40] E. Jakobsson, S.W. Chiu. Stochastic theory of ion movement in channels with single-ion occupancy. Application to sodium permeation of gramicidin channels. *Biophys. J.*, **52**, 33 (1987).
[41] B. Corry, T.W. Allen, S. Kuyucak, S.-H. Chung. Mechanisms of permeation and selectivity in calcium channels. *Biophys. J.*, **80**, 195 (2001).
[42] S. Bek, E. Jakobsson. Brownian dynamics study of a multiply-occupied cation channel: application to understanding permeation in potassium channels. *Biophys. J.*, **66**, 1028 (1994).
[43] W. Im, S. Seefeld, B. Roux. A Grand Canonical Monte Carlo-Brownian Dynamics algorithm for simulating ion channels. *Biophys. J.*, **79**, 788 (2000).
[44] C. Jacoboni, P. Lugli. *The Monte Carlo Method for Semiconductor Device Simulation*, Springer Verlag, New York (1989), pp. 1–356.
[45] T. van der Straaten, G. Kathawala, U. Ravaioli. BioMOCA: A transport Monte Carlo Model for ion channels. *J. Comput. Electron.*, **2**, 2321 (2003).
[46] R. Hockney, J. Eastwood. *Computer Simulation Using Particles*, McGraw-Hill, New York (1981).
[47] S.E. Laux. On particle-mesh coupling in Monte Carlo semiconductor device simulation. *IEEE Trans. CAD Int. Circ. Syst.*, **15**, 1266 (1996).
[48] U. Ravaioli. Vectorization of Monte Carlo algorithms for semiconductor simulation. In *Monte Carlo Device Simulation:*

Full Band and Beyond, K. Hess (Ed.), Kluwer Academic Publishers, Norwell, MA (1991), Ch. 9.
[49] C.J. Wordelman, U. Ravaioli. Integration of a particle–particle–particle-mesh algorithm with the ensemble Monte Carlo method for the simulation of ultra-small semiconductor devices. *IEEE Trans. Electron Dev.*, **47**, 410 (2000).
[50] Boda, D. Private communication
[51] T.A. van der Straaten, G. Kathawala, Z. Kuang, D. Boda, D.P. Chen, U. Ravaioli, R.S. Eisenberg, D. Henderson. Equilibrium structure of electrolyte calculated using equilibrium molecular dynamics, molecular dynamics, and Boltzmann transport Monte Carlo simulations. *Proc. Int. Conf. Comput. Nanosci.*, 447–451 (2003).
[52] D.A. McQuarrie. *Statistical Mechanics*, Harper and Row, New York (1976).
[53] S.R. Berry, S.A. Rice, J. Ross. *Physical Chemistry*, Oxford, New York (2000), p. 1064.
[54] R.L. Rowley. *Statistical Mechanics for Thermophysical Calculations*, Prentice-Hall, Englewood Cliffs, NJ (1994), p. 489.
[55] S.B. Hladky, D.A. Haydon. Discreteness of conductance change in bimolecular lipid membranes in the presence of certain antibiotics. *Nature*, **225**, 451 (1970).
[56] S.B. Hladky, D.A. Haydon. Ion transfer across lipid membranes in the presence of Gramicidin A. I. Studies of the unit conductance channel. *Biochim. Biophys. Acta*, **274**, 294 (1972).
[57] T.W. Allen, O.S. Andersen, B. Roux. Structure of Gramicidin A in a lipid bilayer environment determined using Molecular Dynamics simulations and solid-state NMR data. *J. Am. Chem. Soc.*, **125**, 9868 (2003).
[58] O.S. Andersen, R.E. Koeppe. Molecular determinants of channel function. *Physiol. Rev.*, **72**, S89 (1992).
[59] P.C. Jordan. Microscopic approaches to ion transport through transmembrane channels. The model system Gramicidin. *J. Phys. Chem.*, **91**, 6582 (1987).
[60] J. Leung, R.S. Eisenberg. The effects of the antibiotics Gramicidin A, Amphotericin B, and Nystatin on the electrical properties of frog skeletal muscle. *Biochim. Biophys. Acta*, **298**, 718 (1973).
[61] B.A. Wallace. Gramicidin channels and pores. *Annu. Rev. Biophys. Biophys. Chem.*, **19**, 127 (1990).
[62] Novartis Foundation. *Gramicidin and Related Ion Channel Forming Peptides*, John Wiley, New York (1999).
[63] B. Nadler, U. Hollerbach, B. Eisenberg. The Dielectric Boundary force and its crucial role in Gramicidin. *Phys. Rev. E*, **68**, 021905 1 (2003).
[64] S. Edwards, B. Corry, S. Kuyucak, S.-H. Chung. Continuum electrostatics fails to describe ion permeation in the Gramicidin channel. *Biophys. J.*, **83**, 1348 (2002).
[65] G.H. Golub, C.F. van Loan. *Matrix Computations*, The Johns Hopkins University Press, London (1996).
[66] N.A. Baker, D. Sept, M.J. Holst, J.A. McCammon. The adaptive multilevel finite element solution of the Poisson–Boltzmann equation on massively parallel computers. *IBM J. Res. Develop.*, **45**, 427 (2001).
[67] A. Warshel, S.T. Russell. Calculations of electrostatic interactions in biological systems and in solutions. *Q. Rev. Biol.*, **17**, 283 (1984).
[68] S.T. Russell, A. Warshel. Calculations of electrostatic energies in proteins. The energetics of ionized groups in Bovine Pancreatic Trypsin inhibitor. *J. Mol. Biol.*, **185**, 389 (1985).
[69] C.N. Schutz, A. Warshel. What are the dielectric "constants" of proteins and how to validate electrostatic models? *Proteins*, **44**, 400 (2001).
[70] A. Warshel, A. Papazyan. Electrostatic effects in macromolecules: fundamental concepts and practical modeling. *Curr. Opin. Struct. Biol.*, **8**, 211 (1998).
[71] M.S. Sansom, G.R. Smith, C. Adcock, P.C. Biggin. The dielectric properties of water within model transbilayer pores. *Biophys. J.*, **73**, 2404 (1997).
[72] R. Pomes, B. Roux. Molecular mechanism of H^+ conduction in the single-file water chain of the Gramicidin channel. *Biophys. J.*, **82**, 2304 (2002).
[73] J. Barthel, H. Krienke, W. Kunz. *Physical Chemistry of Electrolyte Solutions: Modern Aspects*, Springer, New York (1998).
[74] S. Durand-Vidal, J.P. Simonin, P. Turq. *Electrolytes at Interfaces*, Kluwer, Boston (2000).
[75] J.-P. Simonin, O. Bernard, L. Blum. Real ionic solutions in the Mean Spherical Approximation. 3. Osmotic and activity coefficients for associating electrolytes in the primitive model. *J. Phys. Chem. B*, **102**, 4411 (1998).
[76] J. Rosgen, B.M. Pettitt, J. Perkyns, D.W. Bolen. Statistical thermodynamic approach to the chemical activities in two-component solutions. *J. Phys. Chem. B*, **108**, 2048 (2004).
[77] S.W. Cowan, T. Schirmer, G. Rummel, M. Steiert, R. Ghosh, R.A. Pauptit, J.N. Jansonius, J.P. Rosenbusch. Crystal structures explain functional properties of two *E. Coli* porins. *Nature*, **358**, 727 (1992).
[78] B. Sakmann, E. Neher. *Single Channel Recording*, Plenum, New York (1995).
[79] S. Aboud, M. Saraniti, R. Eisenberg. Computational issues in modeling ion transport in biological channels: Self-consistent particle-based simulations. *J. Comput. Electron.*, **2**, 239 (2003).
[80] M.P. Allen, D.J. Tildesley. *Computer Simulation of Liquids*, Oxford University Press (1987).
[81] D.R. Lide (Ed.). *CRC Handbook of Chemistry and Physics*, pp. 5–90, CRC press, Boca Raton (1994).
[82] F. Reif. *Fundamentals of Statistical and Thermal Physics*, McGraw-Hill (1987), pp. 565–567.
[83] R.R. Ketchem, W. Hu, T.A. Cross. High-Resolution conformation of Gramicidin-A in a lipid bilayer by solid-state NMR. *Science*, **261**, 1457 (1993).
[84] D.D. Busath, C.D. Thulin, R.W. Hendershot, L.R. Phillips, P. Maughan, C.D. Cole, N.C. Bingham, S. Morrison, L.C. Baird, R.J. Hendershot, M. Cotten, T.A. Cross. Noncontact dipole effects on channel permeation. I. Experiments with (5F-Indole)Trp13 Gramicidin A channels. *Biophys. J.*, **75**, 2830 (1998).
[85] W.L. Jorgensen. OPLS force fields. In *The Encyclopedia of Computational Chemistry*, P.v.R. Schleyer (Ed.), John Wiley & Sons Ltd, Athens, USA (1998).
[86] W.L. Jorgensen, J. Tirado-Rives. The OPLS (Optimized Potentials for Liquid Simulations) potential functions for proteins, energy minimizations for crystals of cyclic peptides and crambin. *J. Am. Chem. Soc.*, **110**, 1657 (1988).
[87] A.D. Mackerell Jr., D. Bashford, M. Bellot, R.L. Dumbrack, M.J. Field, S. Fischer, J. Gao, H. Guo, D. Joseph, S. Ha, L. Kuchnir, K. Kuczera, F.T.K. Lau, C. Mattos, S. Michnick, D.T. Nyugen, T. Ngo, B. Prodhom, B. Roux, B. Schlenkrich, J. Smith, R. Stote, J. Straub, J. Wiorkiewicz-Kuczera, M. Karplus. Self-consistent parameterization of biomolecules for molecular modeling and condensed phase simulations. *Biophys. J.*, **61**, 143 (1992).
[88] V. Fonseca, P. Daumas, F. Ranjalahy-Rasoloarijao, R. Heitz, Y. Lazaro, O.S. Trudelle. Gramicidin channels that have no Tryptophan residues. *Biochemisty*, **31**, 5340 (1992).
[89] O.S. Andersen, D.V. Greathouse, L.L. Providence, M.D. Becker, R.E. Koeppe II. Importance of Tryptophan dipoles for protein function: 5-fluorination of tryptophans in Gramicidin A channels. *J. Am. Chem. Soc.*, **120**, 5142 (1998).